NASA TECHNICAL NOTE

NASA TN D-7652

PARAMETRIC ANALYSIS OF
AN IMAGING RADAR FOR USE AS
AN INDEPENDENT LANDING MONITOR

by W. Thomas Bundick

Langley Research Center
Hampton, Va. 23665

1. Report No. NASA TN D-7652	2. Government Accession No.	3. Recipient's Catalog No.
4. Title and Subtitle PARAMETRIC ANALYSIS OF AN IMAGING RADAR FOR USE AS AN INDEPENDENT LANDING MONITOR		5. Report Date August 1974
		6. Performing Organization Code
7. Author(s) W. Thomas Bundick		8. Performing Organization Report No. L-9322
9. Performing Organization Name and Address NASA Langley Research Center Hampton, Va. 23665		10. Work Unit No. 768-81-02-07
		11. Contract or Grant No.
12. Sponsoring Agency Name and Address National Aeronautics and Space Administration Washington, D.C. 20546		13. Type of Report and Period Covered Technical Note
		14. Sponsoring Agency Code

15. Supplementary Notes

16. Abstract

This report analyzes the capabilities of a real aperture, forward-looking imaging radar for use as an independent landing monitor, which will provide the pilot with an independent means of assessing the progress of an automatic landing during Category III operations.

The analysis shows that adequate ground resolution and signal-to-noise ratio can be obtained to image a runway with grassy surroundings using a radar operating at 35 GHz in good weather and in most fog but that performance is severely degraded in moderate to heavy rain and wet snow. Weather effects on a 10 GHz imager are not serious, with the possible exception of very heavy rain, but the azimuthal resolution at 10 GHz is inadequate with antennas up to 2 m long.

17. Key Words (Suggested by Author(s)) Radar imager Independent landing monitor Landing aid Resolution Forward-looking radar Radar cross section Weather clutter	18. Distribution Statement Unclassified – Unlimited STAR Category 09
19. Security Classif. (of this report) Unclassified	20. Security Classif. (of this page) Unclassified

19. Security Classif. (of this report)	20. Security Classif. (of this page)	21. No. of Pages	22. Price*
Unclassified	Unclassified	71	$3.75

CONTENTS

PRECEDING PAGE BLANK NOT FILMED

PARAMETRIC ANALYSIS OF AN IMAGING RADAR FOR USE

AS AN INDEPENDENT LANDING MONITOR

By W. Thomas Bundick
Langley Research Center

SUMMARY

The development of a suitable independent landing monitor (ILM) may substantially increase pilot acceptance of automatic landings during Category III operations by providing an independent means of assessing the performance of the automatic landing system and the progress of the landing. This report analyzes the capabilities of a real aperture imaging radar for use as such an ILM.

The analysis assumes a set of fixed values, called baseline values, as typical values for certain radar parameters such as receiver noise figure and microwave circuit losses. Other parameters, which include frequency and antenna length, are varied to determine their effect on system performance.

The imaging radar system performance obtained from the analysis is compared with the performance requirements for an imaging type ILM to determine the adequacy of the radar system. However, many of the imaging ILM requirements are not precisely known; so certain requirements, such as signal-to-noise ratio, azimuthal resolution, and weather environment, are assumed or heuristically derived. One critical but somewhat arbitrary assumption was that the radar must perform satisfactorily at a maximum range of 6 km.

The most significant results of the analysis are these: at a range of 6 km, cross-track, or azimuthal, resolutions between 25.7 m and 67.8 m can be obtained with antenna lengths between 1.57 m and 0.761 m (30 in.) at 35 GHz. Adequate resolution (approximately 23 m) at 6 km cannot be obtained at 10 GHz with antenna lengths up to 2 m. At the frequencies examined, sufficient signal-to-noise ratios are achievable in clear weather to adequately image a runway with grassy surroundings, but the same may not be true with snow-covered surroundings. Runway obstructions, such as medium and large aircraft, can be detected at a 6 km range, but light aircraft and small vehicles may not be detected except at shorter ranges. Because of the uncertainties in the differential radar cross section of the targets (grass, etc.) and the uncertainties in the attenuation and reflection characteristics of precipitation, the performance in adverse weather cannot be predicted exactly. However, weather effects on a 10 GHz imager are not serious, with the possible

exception of very heavy rain. The performance of a baseline radar imaging ILM at 35 GHz is limited in rain to rainfall rates of perhaps as small as 0.1 mm/hr. The performance at 35 GHz in wet snow is also seriously degraded. In fog a radar imaging ILM at 35 GHz performs satisfactorily, with the exception of possible slight degradation in very heavy fog.

In summary, the analysis has shown that unless an antenna larger than 2 m can be incorporated into the aircraft, a radar imager operating at 10 GHz is not feasible because of resolution limitations. At 35 GHz a radar imager might be feasible if operation in all weather conditions were not a requirement. These results illustrate that the design of an imaging radar ILM involves a trade-off between frequency and antenna size, and this trade-off results in a compromise between azimuthal resolution and performance in poor weather.

INTRODUCTION

Cancellations and delays in the arrival and departure of commercial airline flights caused by bad weather cost the airlines millions of dollars per year and cause considerable inconvenience to airline passengers. Many of the delays could be significantly reduced, or even eliminated, by using the automatic landing systems which are available on today's new jet transports to effect automatic landings in bad weather, low visibility conditions. These autoland systems are not being used in low visibility conditions, however, for two reasons. First, most airports are not equipped with instrument landing systems (ILS) which can provide sufficiently accurate guidance signals to the aircraft for Category III operation. This problem will eventually be alleviated by the upgrading of the ILS at major U.S. airports and by the development of the microwave landing system (MLS) to replace the ILS in the 1980's. Secondly, the autoland systems have not been accepted by the airline pilots in spite of the fact that thousands of experimental automatic landings have been made successfully. A primary reason for the lack of pilot acceptance is the inability of the pilot to assess the progress of the landing and the performance of the autoland system in conditions of low visibility. It is the function of the independent landing monitor (ILM) to provide the pilot with the information necessary to make this assessment.

In addition to providing the information which will allow the pilot to monitor the performance of the autoland system and the aircraft's situation relative to the runway, several other functions for the ILM have been considered. These include: (1) presentation of sufficient information to allow the pilot to assume control and perform a manual landing in an emergency, (2) detection of obstructions on the runway, (3) presentation of guidance information during roll-out and taxi, and (4) use as a landing aid to reduce weather minimums at airports not equipped with an ILS (or MLS) suitable for making an automatic landing. It is also desirable that the ILM be suitable for use by general aviation as well as by commercial (and military) transports.

2

The function of the ILM is not the only unanswered philosophical question. For example, what is the degree of independence of the ILM from the ILS and other ground equipments? What is the degree of independence from other aircraft systems? Under what weather conditions should the ILM be required to operate? As important as these questions are, they are beyond the scope of this paper. Rather than philosophy, this paper will address one form of implementation of the ILM, namely, imaging radar.

Various sensors operating in different areas of the electromagnetic spectrum have been considered for use in an ILM. They include imaging radars (refs. 1 and 2), monopulse radar (ref. 3), active/passive microwave radiometers, low-light level television, and infrared devices. Some of these techniques have been implemented and tested, and studies (ref. 4) have been conducted to determine the display requirements for an ILM. Although these studies may not be conclusive, the use of a real world perspective display, such as might be obtained from an imaging radar, has received strong support from pilots (ref. 5).

It is the purpose of this paper to present the results of a parametric study conducted to evaluate the potential of real aperture imaging radar to provide such a real world display for an ILM. The study analyzes the effects of radar parameters such as transmitter power, antenna size, frequency, and pulse duration; the effects of target backscatter properties; and the effects of rain, snow, and fog on the capabilities of the system to provide an image of specified quality and information content which might be suitable for use in an ILM.

SYMBOLS AND NOTATIONS

A   physical antenna area, $meters^2$

A_e effective antenna area, $meters^2$

b   length of side of corner reflector, meters

C   clutter power, watts

c   speed of light, 3×10^8 meters/second

D   visibility, meters

dBsm   decibel relative to 1 $meter^2$

F   receiver noise figure

f   frequency, hertz

$f(P)$ probability density function of P

f_c carrier frequency, hertz

f_d doppler frequency, hertz

f_1 lower limit of doppler frequency from a resolution element, hertz

f_2 upper limit of doppler frequency from a resolution element, hertz

Δf doppler bandwidth, hertz

G   antenna gain

h   altitude, meters

$$K = \frac{m^2 - 1}{m^2 + 2}$$

K_a-band   26.5 GHz to 40.0 GHz

k   Boltzmann constant, 1.380×10^{-23} joules/K

L   microwave circuit losses

ℓ antenna length, meters

M   mass of condensed water per unit volume of air, grams/meter^3

m   complex refractive index of water

N   random variable denoting noise voltage after integration, volts

N_I number of pulses integrated

N_R number of pulses received during the time the antenna scans one beamwidth

N_i random variable denoting noise voltage before integration, volts

4

P random variable denoting received power, watts

P_R mean value of received power, watts

P_t transmitter power, watts

P_ρ power received from a resolution element, watts

p pulse repetition frequency, pulses/second

R range, meters

$R_{vv}(\tau)$ correlation function of video signal from a resolution element

R_1, R_2 range to near and far edges, respectively, of a resolution element, meters

r rainfall rate, millimeters/hour

$S(t)$ random process denoting predetection signal received from a resolution element, volts

$S_{dd}(\omega)$ postdetection power spectral density of doppler, watts/radian-second^{-1}

$S_{pp}(\omega)$ predetection power spectral density of doppler, watts/radian-second^{-1}

$S_{vv}(\omega)$ postdetection power spectral density of doppler after filtering, watts/radian-second^{-1}

$(SCR)_T$ signal-to-clutter ratio where clutter is produced by random fluctuations in return from target

$(SCR)_W$ signal-to-clutter ratio where clutter is produced by random fluctuations in return from weather

SNR signal-to-noise ratio

$(SNR)_\rho$ signal-to-noise ratio of signal from a resolution element

s antenna scan rate, scans/second

T	reference temperature, 293 K
t	time, seconds
t_I	integration time, seconds
$t_{I,max}$	maximum integration time, seconds
V	random variable denoting signal voltage after integration, volts
V(t)	random process denoting envelope of received signal, volts
V_i	random variable denoting postdetection signal from single pulse, volts
V_ρ	volume of clutter cell, meters^3
v	aircraft velocity, meters/second
w	antenna height (elevation dimension), meters
X-band	8.2 GHz to 12.4 GHz
x,y	Cartesian coordinates of resolution element, meters
Z	effective reflectivity factor of rain, millimeters^6/meter^3
α	attenuation coefficient, decibels/meter
β	antenna depression angle, radians
γ	radar cross section per unit projected area, meters^2/meter^2
γ_v	glideslope, radians
ζ	elevation angle of aircraft as viewed from far end of runway, radians
η	antenna efficiency
θ	incidence angle, radians

6

$\theta(t)$ random process denoting phase of received signal, radians

θ_a antenna along-track (elevation) beamwidth, radians

θ_c antenna cross-track (azimuth) beamwidth, radians

λ wavelength, meters

ρ resolution element, meters^2

ρ_a along-track (radial) resolution, meters

ρ_c cross-track (azimuthal) resolution, meters

$\rho_{vv}(\tau)$ correlation coefficient of postdetection doppler signal after filtering

ρ_w density of water, grams/centimeter^3

Σ radar clutter cross section (reflectivity) of precipitation per unit volume, meters^2/meter^3

σ radar cross section, meters^2

σ_N standard deviation of postintegration noise, volts

$\sigma_{N,i}$ standard deviation of preintegration noise, volts

σ_P standard deviation of received power, watts

σ_V standard deviation of postintegration signal, volts

$\sigma_{V,i}$ standard deviation of preintegration (single pulse) signal, volts

$\sigma_o, \sigma_o(\theta)$ differential radar cross section, meters^2/meter^2

τ time variable, seconds

τ_p pulse duration, seconds

τ_{90}	time when correlation coefficient equals 0.9, seconds
ϕ	antenna scan angle, radians
ϕ_L	width of antenna scan, radians
Ω	one-half of doppler bandwidth, radians/second
ω	frequency, radians/second
ω_c	carrier frequency, radians/second
ω_d	doppler frequency, radians/second
ω'	dummy frequency variable, radians/second

Special mathematical notation:

$E\{\cdot\}$	statistical expected value
$\dot{R}$	dot over a variable denotes derivative with respect to time
$\overline{V}$	bar over a variable denotes statistical mean value
$*$	convolution

BASELINE SYSTEM

The geometrical relationships between the aircraft radar antenna and the airport scene are depicted in figure 1, where the aircraft is shown over the extended center line of the runway and on the proper glide slope. As with side-looking real aperture imaging radars, the antenna beam is elliptical with the beam being narrow in the azimuthal direction. This narrow beamwidth is necessary so that sufficient cross-track resolution is obtained. Resolution along track is achieved by ranging so the antenna beam is sufficiently broad in elevation to illuminate all ranges of interest. To cover all of the ground area of interest in the azimuthal direction, the antenna is electronically or mechanically scanned in that direction.

A simplified block diagram of the system is shown in figure 2. A pulse of duration τ_p is transmitted and reflected by the ground. The return signal is detected and
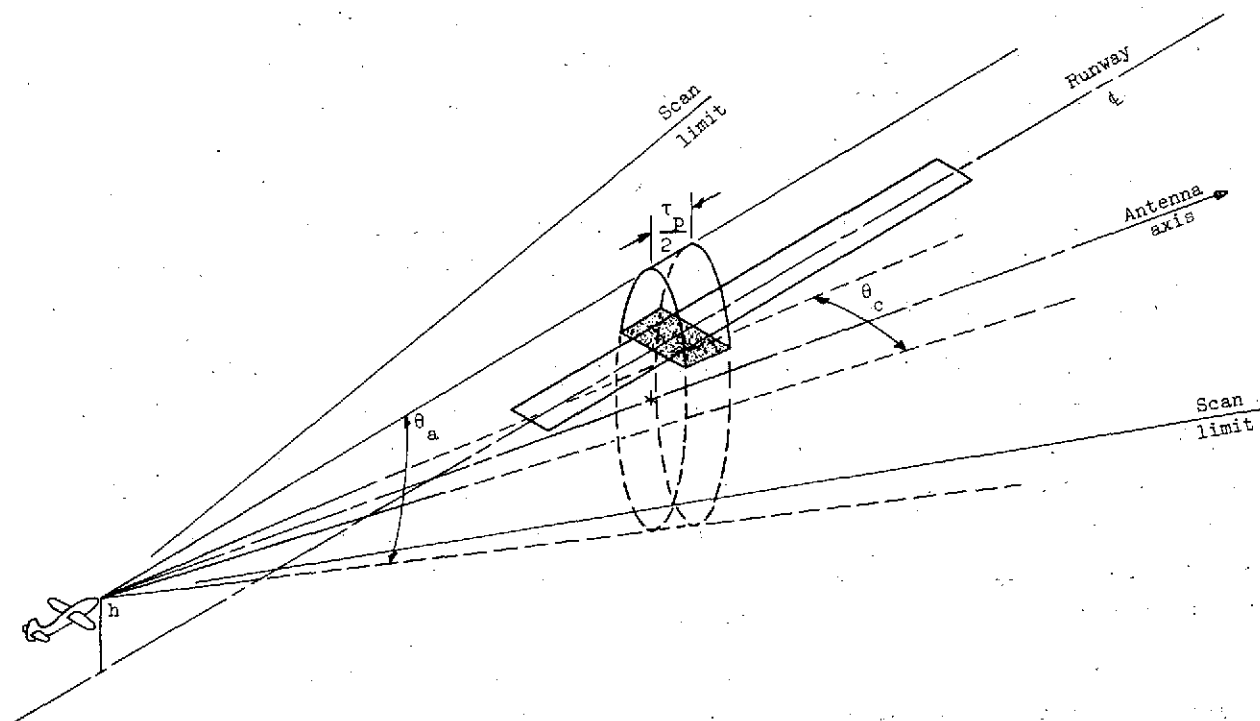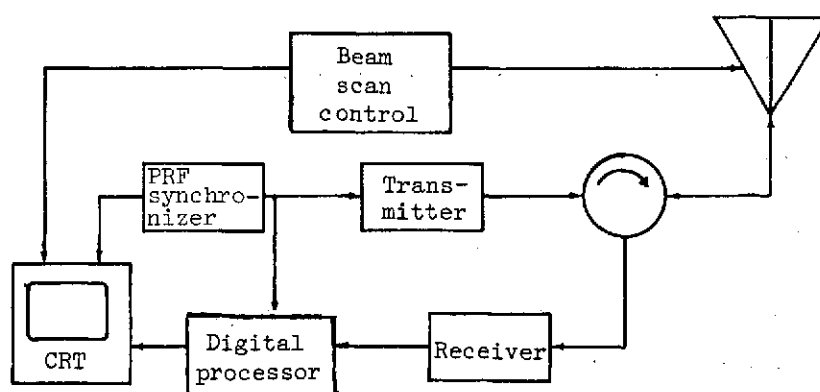
8

Figure 1.- ILM geometry.

Figure 2.- Simplified block diagram.

used to modulate the intensity of a CRT (cathode-ray tube) display, whose sweep in the vertical direction is synchronized with the transmitter PRF (pulse repetition frequency) and in the horizontal direction with the antenna scan. The variation in the backscatter properties of the airport scene produces an image of the scene on the CRT display. Since a radar image is normally produced in range-angle coordinates, some processing of the data is required to convert the image to angle-angle coordinates. Though this processing adds some complexity to the system, it does not affect the basic capabilities of the radar and will not be considered further.

Before proceeding with the analysis, a set of values will be established for certain radar parameters which will be kept constant for the numerical calculation throughout the report. For the along-track (elevation) beamwidth (field of view) θ_a, previous ILM studies and implementations have used values of 17° (ref. 1), 18°, and 30° (ref. 2). In the current study, a value of 17° will be used. It will be assumed that the antenna is pointed at a depression angle of 6.5^O such that the field of view in elevation is from -2^O to 15° depression with respect to the horizontal.

As will be shown, the cross-track resolution is inversely proportional to frequency while the degradation in radar performance caused by weather effects increases with frequency. Thus frequencies of 10 GHz, 15 GHz, and 35 GHz were chosen because they span the frequency region of reasonable compromise between resolution and weather effects.

Antenna scan limits of $\pm 15^O$ (ref. 2), $\pm 16.5^O$ (ref. 2), and $\pm 20^O$ have been considered, while scan rates have varied from 2.5 per sec (ref. 1) to 10 per sec (ref. 2). For this study, scan limits of $\pm 15^O$ and a scan rate of 5 per sec were chosen.

The above chosen values and values considered typical of the other parameters for the baseline system are listed in table I.

TABLE I.- BASELINE VALUES OF RADAR PARAMETERS

Transmitter peak power, P_t, kW 50

Frequency, f, GHz 10, 15, 35

Wavelength, λ, cm 3, 2, 0.857

Pulse duration, τ_p, μsec 0.1

System noise figure, F, dB 10

Microwave circuit losses, L, dB . . . . -1.5

Antenna efficiency, η 0.65

Antenna beamwidth (elevation), θ_a, deg 17

Antenna scan width (azimuth), ϕ_L, deg 30

Antenna scan rate, s, sec^{-1} 5

PARAMETRIC ANALYSIS

The ILM is required to operate with two types of targets, which may be classified as area and discrete. Area targets are targets which are homogeneous and large compared to the radar resolution. These targets, such as runways, taxiways, and their surroundings, must be imaged by the radar with sufficient fidelity to allow the pilot to determine the aircraft's position relative to the runway. The discrete targets, which may be considerably smaller than a resolution element, are important for two reasons. First, it is imperative that runway obstructions, such as ground vehicles and other aircraft, be detected by the pilot sufficiently early in the approach to permit a go-around. Second, the detection of runway and approach lights would enhance the image of the runway.

Area Targets

Resolution.- The cross-track (azimuth) resolution ρ_c on the ground is determined for a real aperture radar by the azimuth beamwidth θ_c according to equation (1). (See fig. 3.)

$$\rho_c \approx R\theta_c \qquad \left(\text{for} \quad \theta_c \ll 1\right) \qquad (1)$$

Figure 3.- Resolution geometry.

In the along-track direction the resolution ρ_a is a function of the pulse width and the incidence angle θ or the depression angle β, assuming a flat earth,

$$\rho_a = \frac{c\tau_p \csc \theta}{2} = \frac{c\tau_p \sec \beta}{2} \tag{2}$$

For depression angles near zero, equation (2) reduces to

$$\rho_a \approx \frac{c\tau_p}{2} \qquad \text{(for } \beta \ll 1\text{)} \tag{3}$$

This approximation is good for the radar imaging ILM at the longer ranges. A resolution element ρ is the product of the cross-track and along-track resolutions

$$\rho = \rho_c \rho_a = \frac{c\tau_p R\theta_c \sec \beta}{2} \approx \frac{c\tau_p R\theta_c}{2} \qquad \left(\text{for } \theta_c, \beta \ll 1\right) \tag{4}$$

Consider now the cross-track resolution. For an antenna length ℓ in the cross-track dimension the beamwidth may be approximated by (ref. 6, p. 9-5)

$$\theta_c \approx \frac{\lambda}{\ell} \tag{5}$$

In figure 4 the azimuth beamwidth is plotted as a function of ℓ for frequencies of 10 GHz, 15 GHz, and 35 GHz.

The cross-track resolution, as expressed by equation (1), is plotted in figure 5 as a function of antenna beamwidth for ranges of 1, 2, 3.66, and 6 km. (A range of 3.66 km is equivalent to the length of a 12 000 ft runway.) Reference to figures 4 and 5 will show the relationship between antenna length and cross-track resolution at the specified frequencies and ranges.

Suppose it is desired to have a cross-track resolution of 20 m at a range of 3.66 km. Combining equations (1) and (5) produces the following expression for resolution:

$$\rho_c = \frac{R\lambda}{\ell} \tag{6}$$

Then at 35 GHz an antenna length of 1.57 m is needed to obtain the desired resolution. In figure 6 is plotted the resolution as a function of range for antenna lengths of 0.761 m (30 in.) and 1.57 m. (A length of 0.761 m (30 in.) was chosen as typical of airborne antennas.) These two antenna sizes will be used again later in the analysis.

Required resolution.- A search of the literature, admittedly brief and nonexhaustive, failed to produce any information concerning previous research that directly addressed the question of what is the required ground resolution for an imaging type ILM. Since the
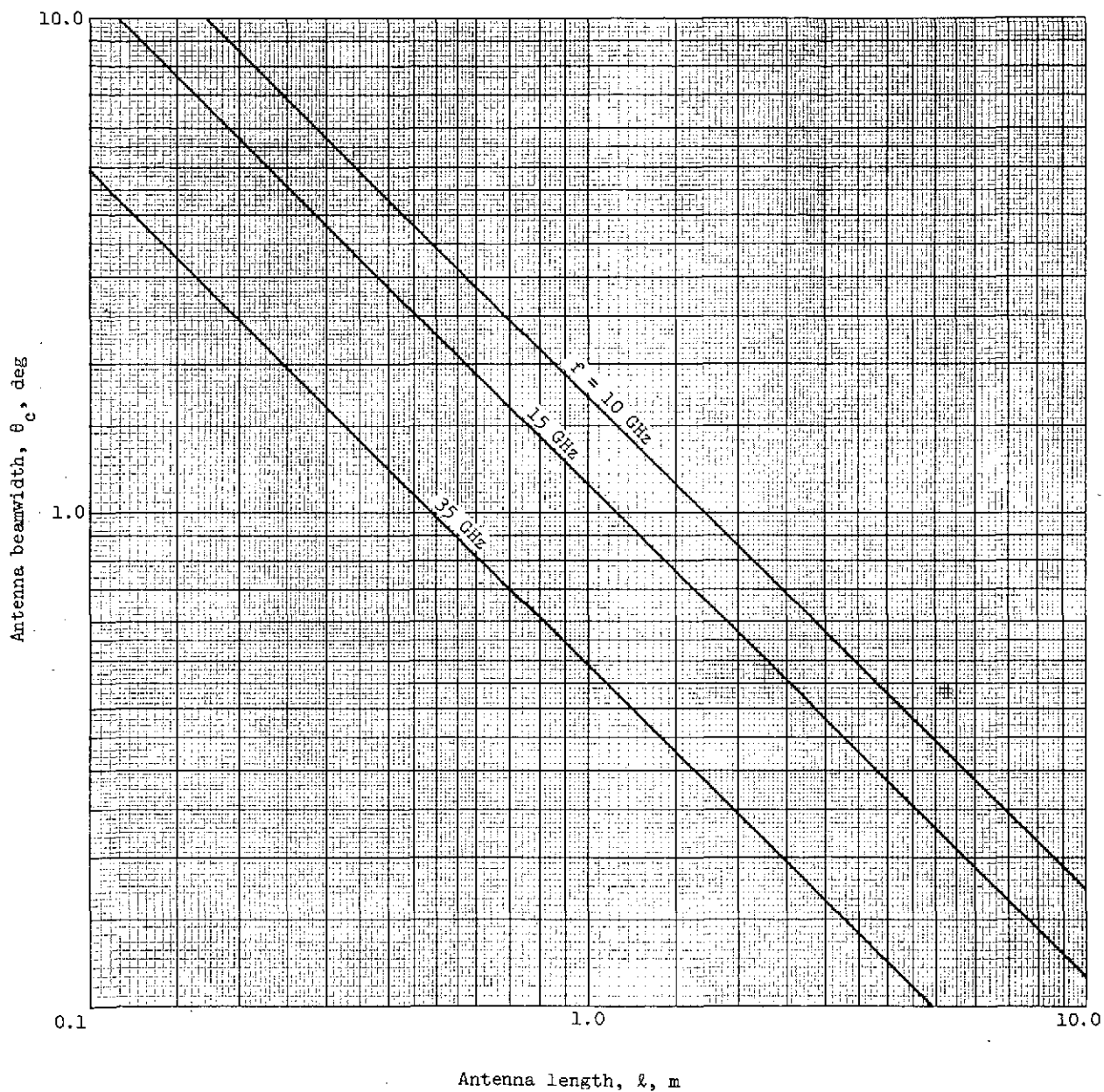
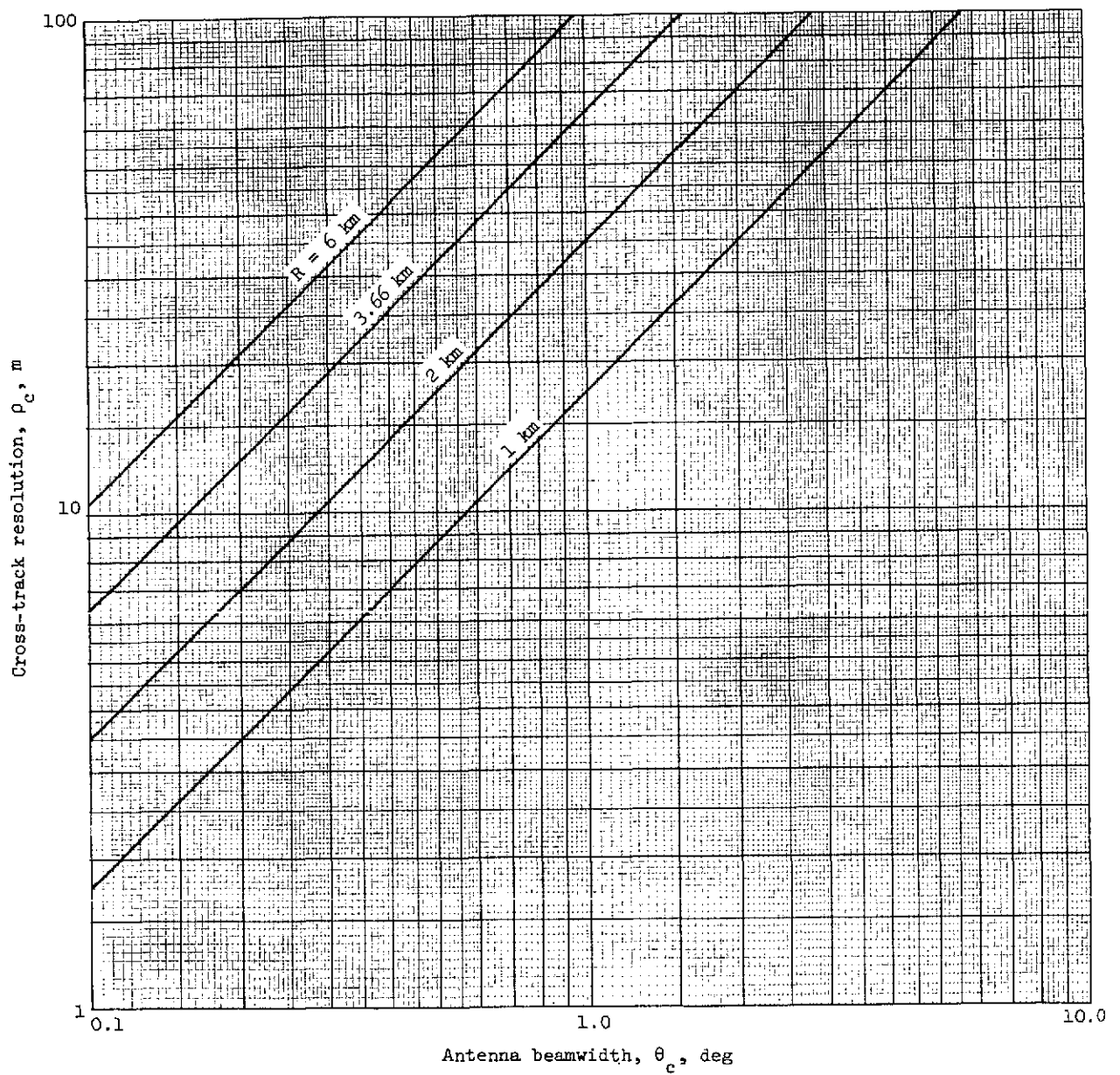Figure 4.- Cross-track beamwidth versus antenna length.
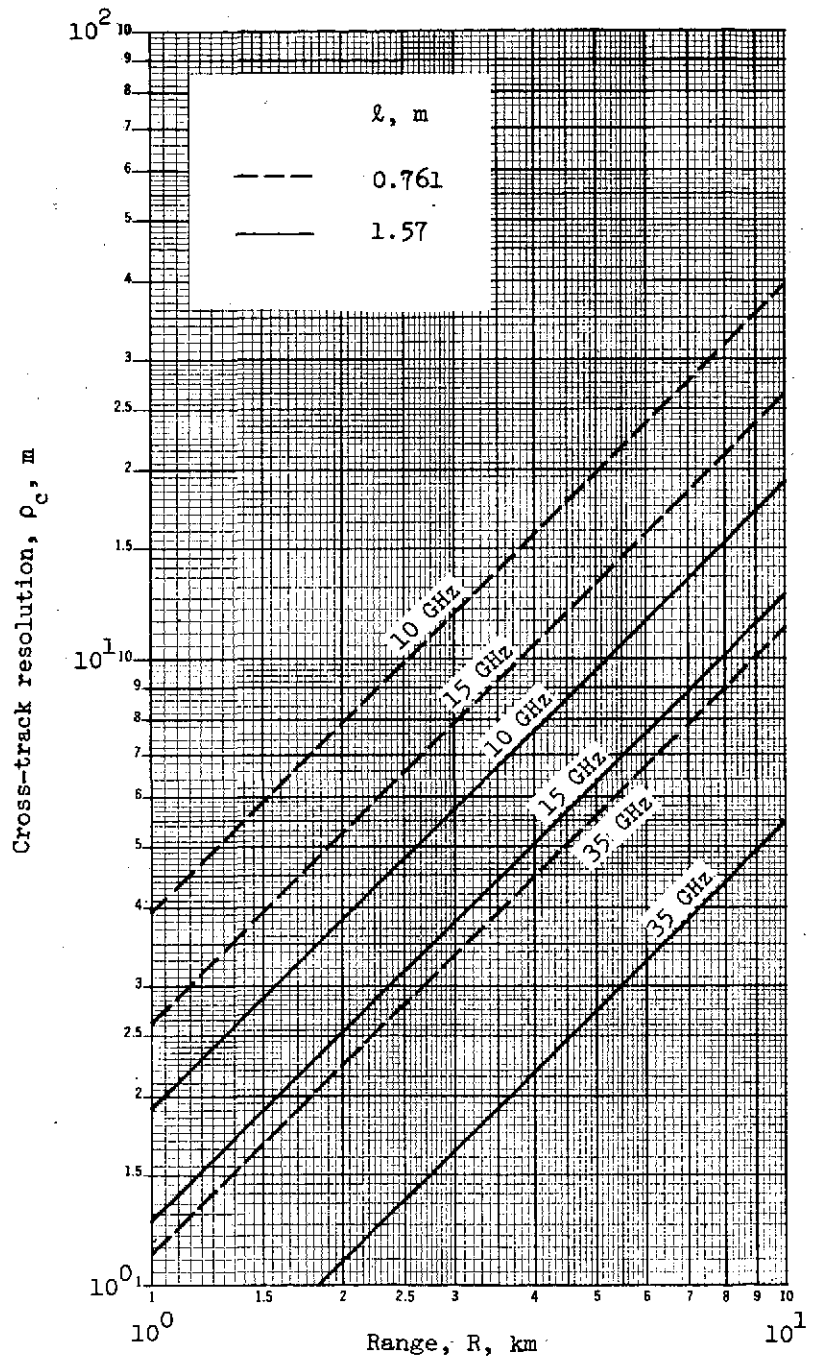
Figure 5.- Cross-track resolution versus beamwidth.

Figure 6.- Cross-track resolution versus range.

required resolution apparently has not been determined, a value for this requirement will be assumed.

At the maximum operating range, an imaging ILM will be used to detect the presence of the runway and to provide gross alinement information. Let it be assumed that for detection purposes the cross-track resolution ρ_c should be equivalent to not more than one-half the runway width. Then for a typical runway width of 45.7 m (150 ft) the cross-track resolution at maximum range should be around 23 m.

At shorter ranges as the aircraft gets closer to touchdown, much more precise alinement and altitude information must be obtainable from the ILM image, and the resolution requirements become considerably more stringent, but are not exactly known. If the resolution requirement of 23 m is to be achieved at the previously assumed maximum range of 6 km, then the radar imaging ILM must have a cross-track beamwidth θ_c of 0.22° (from eq. (1)). With this beamwidth and at a range of 583 m, corresponding to the range to touchdown from an altitude of 30.5 m (100 ft), the cross-track resolution ρ_c would be 2.2 m, which is much better than the along-track resolution of the baseline system.

Henceforth, a resolution requirement of 23 m at maximum range will be assumed, but it must be emphasized that this requirement has not been verified experimentally.

Consider a resolution element ρ at a range R as in figure 3. From the radar equations the power received by the radar after reflection by the ground element ρ is given by equation (7)

$$P_\rho = \frac{P_t L^2 G \sigma A_e}{\left(4\pi R^2\right)^2} \tag{7}$$

where

P_ρ power received from a resolution element, W

P_t transmitter power, W

L microwave circuit losses

G antenna gain

σ radar cross section of ρ, m^2

A_e effective area of antenna, m^2

R range, m

16

If the ground element ρ is homogeneous and small enough that the incidence angle θ is relatively constant, then the cross section can be expressed as the product of the element area ρ and the average backscatter cross section $\sigma_o(\theta)$, sometimes called the differential scattering cross section,

$$\sigma = \rho\sigma_o(\theta) \tag{8}$$

Upon substitution for σ, equation (7) becomes

$$P_\rho = \frac{P_t L^2 G A_e \rho\sigma_o(\theta)}{\left(4\pi R^2\right)^2} \tag{9}$$

From equation (9) it can be seen that the power received from a ground resolution element, and thus the signal-to-noise ratio, is directly proportional to the differential cross section σ_o. Furthermore, it will later be shown that the signal-to-clutter ratio during bad weather operation is also directly proportional to σ_o. Therefore, before proceeding with the performance analysis, let us pause to consider the range of differential cross sections that are applicable to the ILM problem.

Differential radar cross section.- The differential radar cross section is a function of the incidence angle, the frequency, and, of course, the target. The targets of interest for the radar imaging ILM are the runway and its surroundings, which include concrete, bare ground, grass, weeds, snow, and water. A number of measurements of σ_o have been made for various targets (ref. 6, ch. 25), but much of the data is not applicable to the ILM because the appropriate incidence angles are not included.

With an elevation beamwidth θ_a of 17° and assuming the upper limit is 2^O above the horizontal, the incidence angles of interest lie between 75° and 90°. Table II is a tabulation of measurements of σ_o for linear polarization taken by Cosgriff, Peake, and Taylor (ref. 7) and by Grant and Yaplee (ref. 8). Note that the data in reference 7 are plotted as γ versus grazing angle, which is the complement of θ. Since γ is the cross section per unit projected area (surface area projected onto a plane perpendicular to the direction of propagation), σ_o is found by multiplying γ by $\cos\theta$. The data in table II are for an incidence angle of 80°. Data for an incidence angle between 85° and 90° would be useful but are unavailable. To facilitate a comparison of the cross sections of the concrete runway and its surroundings, the tabulated data are shown graphically in figure 7.

From figure 7 it can be seen that the cross section is a function of frequency and is smaller at X-band than at K_a-band. Furthermore, the cross section varies considerably for the runway surroundings. As an estimate of the minimum cross section for use in later numerical calculations, values of -26 dB and -33 dB for K_a-band and X-band, respectively, will be used for the runway surroundings at $\theta = 80^O$. For the runway -34 dB

TABLE II.- RADAR CROSS SECTION OF VARIOUS

TERRAIN TYPES AT $\theta = 80^{\circ}$

Terrain type (a)	Cross section, σ_o, dB			
	X-band		K_a-band	
	Horizontal polarization	Vertical polarization	Horizontal polarization	Vertical polarization
Cosgriff, Peake, and Taylor (ref. 7)				
Concrete	-53	-43	-43	-32
Concrete	-54	-50	-46	-34
Disked ground	-33	-32	-22	-23
Plowed field	-24	-26	-33	-31
Green grass, 1 in.			-26	-26
Green grass, 1 in.			-22	-23
Green grass, 1 in.			-18	-18
Green grass, 2 in.	-31	-25	-19	-22
Green grass, 2 in.	-32	-33	-22	-22
Green grass, 2 in.	-32	-32		
Green grass, 2 in.	-31	-27		
Green grass, 2-3/4 in.			-20	-20
Green grass, 8 in. flattened to 3 in.			-25	-25
Green grass, 15 in.	-21	-21	-18	-20
Brown grass, 1 in.	-32	-31		
Green wheat, 1/2 in.	-35	-38	-23	-26
Green wheat, 2 in.	-33	-30		
Wheat stubble, 12 in.	-26	-27	-20	-21
Alfalfa and grass, 6 in.	-33	-32		
Green grass, 1 in.	-31		-26	
Green grass, 1 in., with snow, 1 in.	-41		-39	
Green grass, 1 in., with snow, 4 in.	-36		-44	
Grant and Yaplee (ref. 8)				
Short dry grass and weeds		-18		-18
Sandy loam partially covered with short dry grass		-19		-27
Wet sandy loam partially covered with short green grass		-12		-18
Marsh, sand, and bushes		-21		-14

[a]Several values of cross section are shown for the same type of terrain because measurements were made at different locations or times.
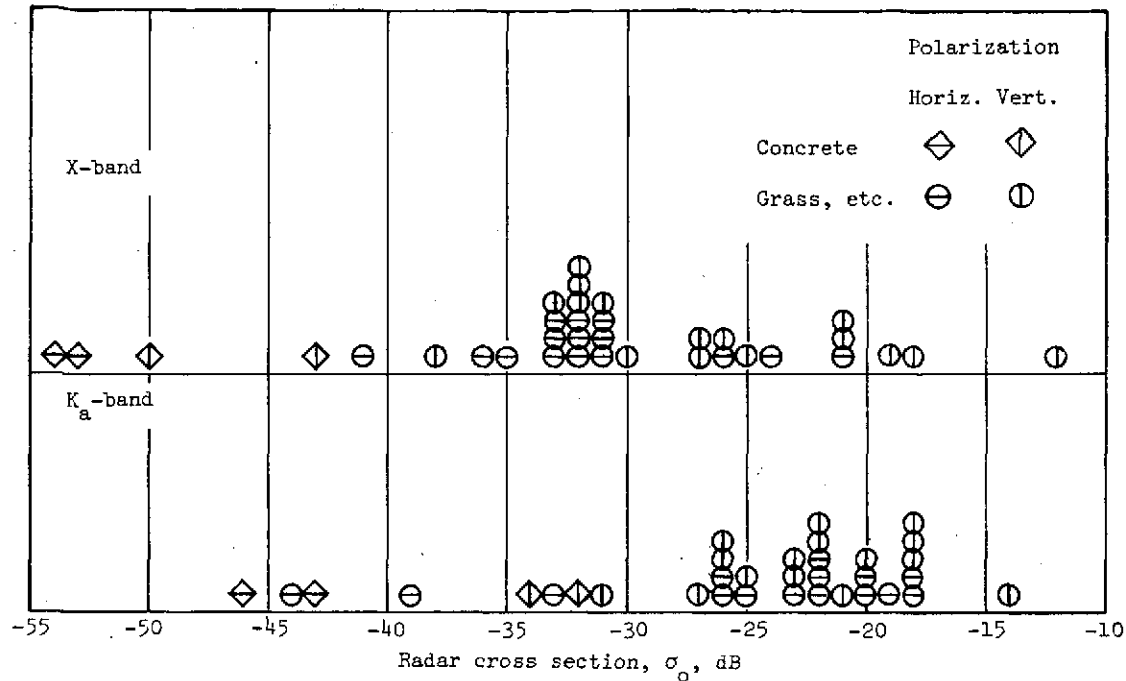
Figure 7.- Radar cross section at $\theta = 80^\circ$.

and -50 dB will be used. These values should decrease at greater incidence angles, but, as previously mentioned, measured data are not available. The measurements of γ by Cosgriff, Peake, and Taylor (ref. 7) show that γ is relatively constant as a function of incidence angle for many grassy type terrains. Therefore, as a best guess, σ_o for angles of incidence greater than 80° will be computed from the value at $\theta = 80^\circ$ as follows:

$$\sigma_o(\theta) = \sigma_o\left(80^\circ\right)\frac{\cos \theta}{\cos 80^\circ} \tag{10}$$

This procedure may produce estimates of $\sigma_o(\theta)$ that are slightly large for specular targets such as concrete and snow, but these approximations are the best available.

Consider the case shown in figure 8 where the aircraft is on a 3° glide slope and at a range of 6 km from the far end of the runway. The incidence angle θ at a range R is found as follows: From the law of sines

$$\sin\left(3^\circ - \zeta\right) = \frac{3.66}{6} \sin 177^\circ$$

$$\zeta = 1.17^\circ \tag{11}$$

From the properties of right triangles

$$h = 6 \sin \zeta = 0.122 \text{ km} \tag{12}$$

19

Figure 8.- Geometry at maximum range.

and

$$\theta = \text{arc cos } \frac{h}{R} \tag{13}$$

With θ calculated from equation (13) and with $\sigma_o(80°)$ equal to -33 dB and -26 dB at X-band and K_a-band, respectively, $\sigma_o(\theta)$ for grass, weeds, etc. can be computed using equation (10). Results are listed in table III. Also tabulated are measurements of $\sigma_o(\theta)$. for undisturbed snow reported in reference 9.

TABLE III.- ESTIMATED MINIMUM RADAR CROSS SECTION

FOR RUNWAY SURROUNDINGS

Range, R, km	Incidence angle, θ, deg	$\dfrac{\cos \theta}{\cos 80°}$, dB	Cross section for grass, etc., $\sigma_o(\theta)$, dB		Cross section for snow, $\sigma_o(\theta)$, dB (ref. 9)			
					X-band		K_a-band	
			X-band	K_a-band	Horizontal polarization	Vertical polarization	Horizontal polarization	Vertical polarization
1	83.0	-1.5	-34.5	-27.5	---	---	---	---
3	87.7	-6.3	-39.3	-32.3	---	---	---	---
5	88.6	-8.5	-41.5	-34.5	---	---	---	---
7	89.0	-10.0	-43.0	-36.0	-48	-56	---	---
9	89.2	-11.1	-44.1	-37.1	-52	-59	---	-53
10	89.3	-11.5	-44.5	-37.5	-54	-61	-51	-53

It should be noted that the reflected signal is a random process. The fluctuating signal amplitude is described by Rayleigh statistics, and therefore the received power is exponentially distributed. The cross section σ_o is used to compute the mean value of the return.

Signal-to-noise ratio.- From equation (9) the mean power received from a ground resolution element ρ is given by

$$P_\rho = \frac{P_t L^2 G A_e \rho \sigma_o(\theta)}{\left(4\pi R^2\right)^2}$$

Rearrange equation (9) as follows: The antenna gain and effective aperture can be expressed in terms of the physical aperture A of the antenna; that is,

$$G = \frac{4\pi\eta A}{\lambda^2} \tag{14}$$

$$A_e = \eta A \tag{15}$$

where η is the antenna efficiency. But,

$$A = \ell w \tag{16}$$

where ℓ is the antenna length (azimuth dimension) and w is the antenna height (elevation dimension). Furthermore,

$$w = \frac{\lambda}{\theta_a} \tag{17}$$

Substitution of equations (4) and (14) through (17) into equation (9) produces

$$P_\rho = \frac{P_t L^2 \eta^2 \ell^2 \rho_a \rho_c \sigma_o}{4\pi R^4 \theta_a^2} \tag{18}$$

Assuming an IF bandwidth of $1/\tau_p$ and noise figure F, the mean predetection signal-to-noise ratio of the return from a resolution element is

$$(SNR)_\rho = \frac{P_t L^2 \eta^2 \ell^2 \rho_a \rho_c \sigma_o \tau_p}{4\pi R^4 \theta_a^2 kTF} \tag{19}$$

Fixed beamwidth: Consider the signal-to-noise ratio as a function of range for a fixed antenna beamwidth. Rewrite equation (19) with ρ_a and ρ_c in terms of τ_p and θ_c, respectively,

$$(SNR)_\rho = \frac{P_t L^2 \eta^2 \lambda^2 \sigma_o \tau_p^2 c}{8\pi R^3 \theta_a^2 \theta_c kTF} \tag{20}$$

Let τ_p equal 0.1 μsec corresponding to a resolution of 15 m, and let $\theta_c = 0.00547$ rad (0.313^o), which produces a resolution of 20 m at a range of 3.66 km (12 000 ft). Using the baseline values from table I, the signal-to-noise ratio in dB is

$$(\text{SNR})_\rho = 198.3 + 20 \log \lambda + 10 \log \sigma_0 - 30 \log R \tag{21}$$

Equation (21) is plotted in figure 9 using values for σ_0 of -33 dB and -26 dB at X-band and K_a-band, respectively.

To account for the change in σ_0 as a function of range due to changing incidence angle, the signal-to-noise ratio from equation (21) is also plotted in figure 9 using values of $\sigma_0(\theta)$ for grass taken from table III.

Fixed antenna length: In the preceding section the signal-to-noise ratio was computed for a fixed beamwidth of 0.313°. To achieve this beamwidth at 10 GHz requires an antenna length of 5.49 m (18.0 ft). Now consider the SNR for a fixed antenna length. Equation (20) can be rewritten as

$$(\text{SNR})_\rho = \frac{P_t L^2 \eta^2 \lambda \ell \sigma_0 \tau_p^2 c}{8\pi R^3 \theta_a^2 kTF} \tag{22}$$

Using the baseline values, equation (22) becomes in dB

$$(\text{SNR})_\rho = 175.7 + 10 \log \lambda + 10 \log \ell + 10 \log \sigma_0 - 30 \log R \tag{23}$$

Using equation (23), the SNR is plotted in figure 10 as a function of range for antenna lengths of 0.761 m (30 in.) and 1.57 m using $\sigma_0(80^\circ)$ and using $\sigma_0(\theta)$ from table III.

Fixed range: Let the range be fixed at 6 km. In order to estimate the signal-to-noise ratio of the return from different targets, consider the SNR as a function of cross section σ_0. For R = 6 km, equation (23) becomes

$$(\text{SNR})_\rho = 62.4 + 10 \log \lambda + 10 \log \ell + 10 \log \sigma_0 \tag{24}$$

The predetection SNR, as calculated from equation (24), is plotted in figure 11 as a function of cross section. Also shown in figure 11 is the postdetection signal-to-noise ratio assuming a square-law detector.

The postdetection signal-to-noise ratio as used in this report is defined as the ratio of the average (dc) detector output power with a signal plus noise input to the ac detector output power (noise variance) with noise only at the input. With this definition the postdetection signal-to-noise ratio is approximately equal to the square of the input signal-to-noise ratio. Since this is not the usual relationship, a brief development is shown below based on the work of Panter (ref. 10). In the notation of reference 10, let the output current I of the square law detector be related to the input voltage V by the relationship
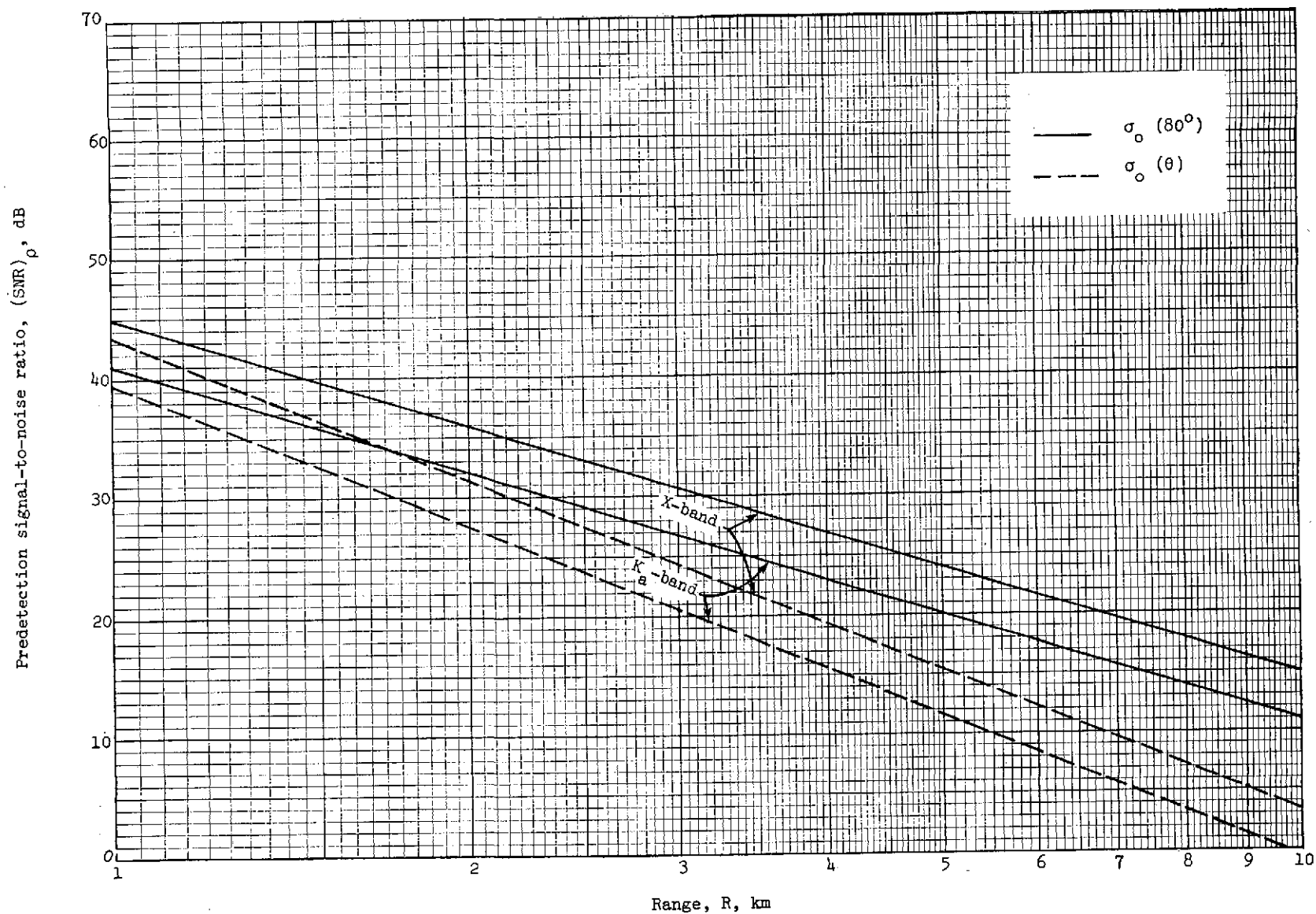
$$I = aV^2 + bV \tag{25}$$

22

Figure 9.- SNR for constant beamwidth.
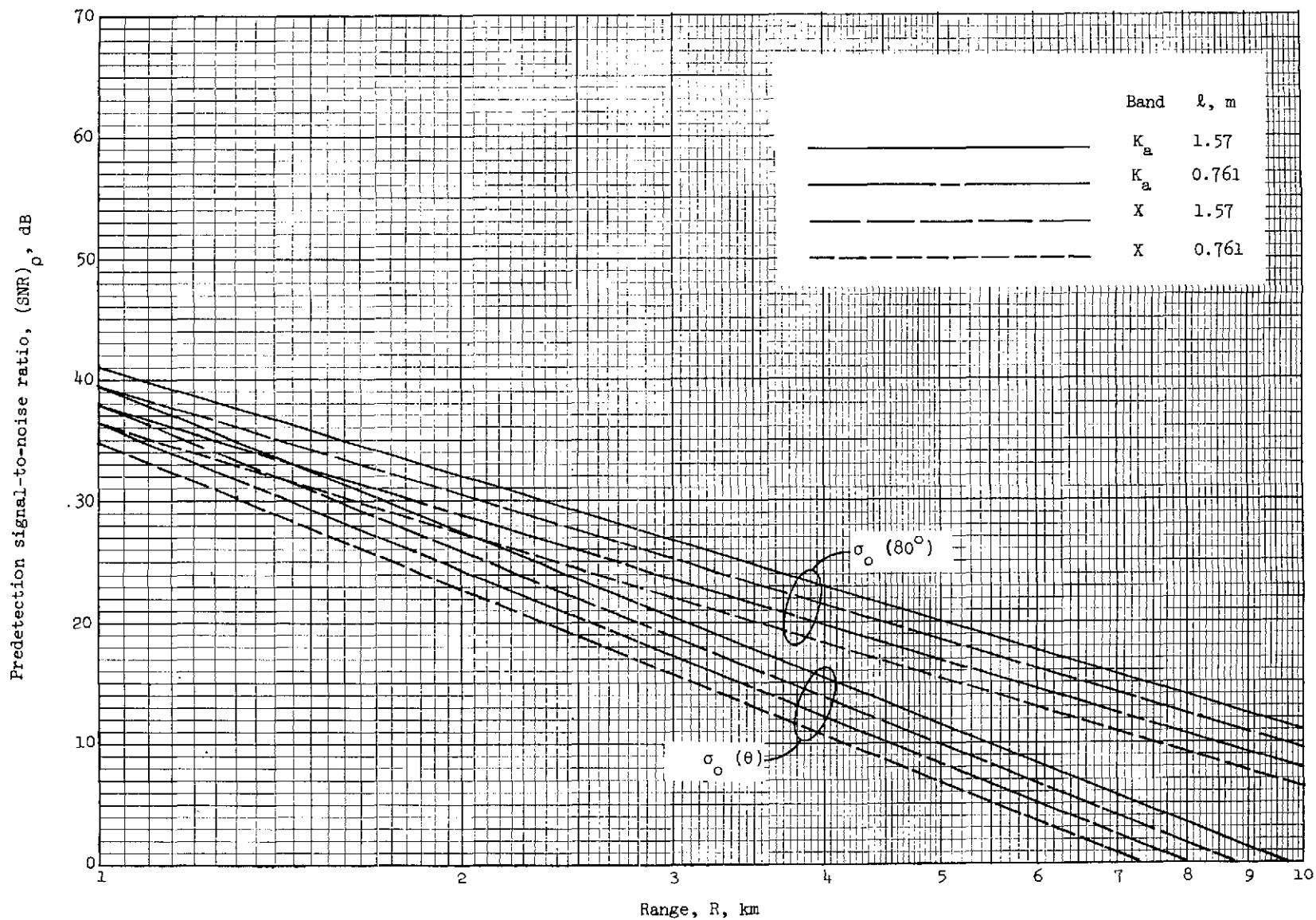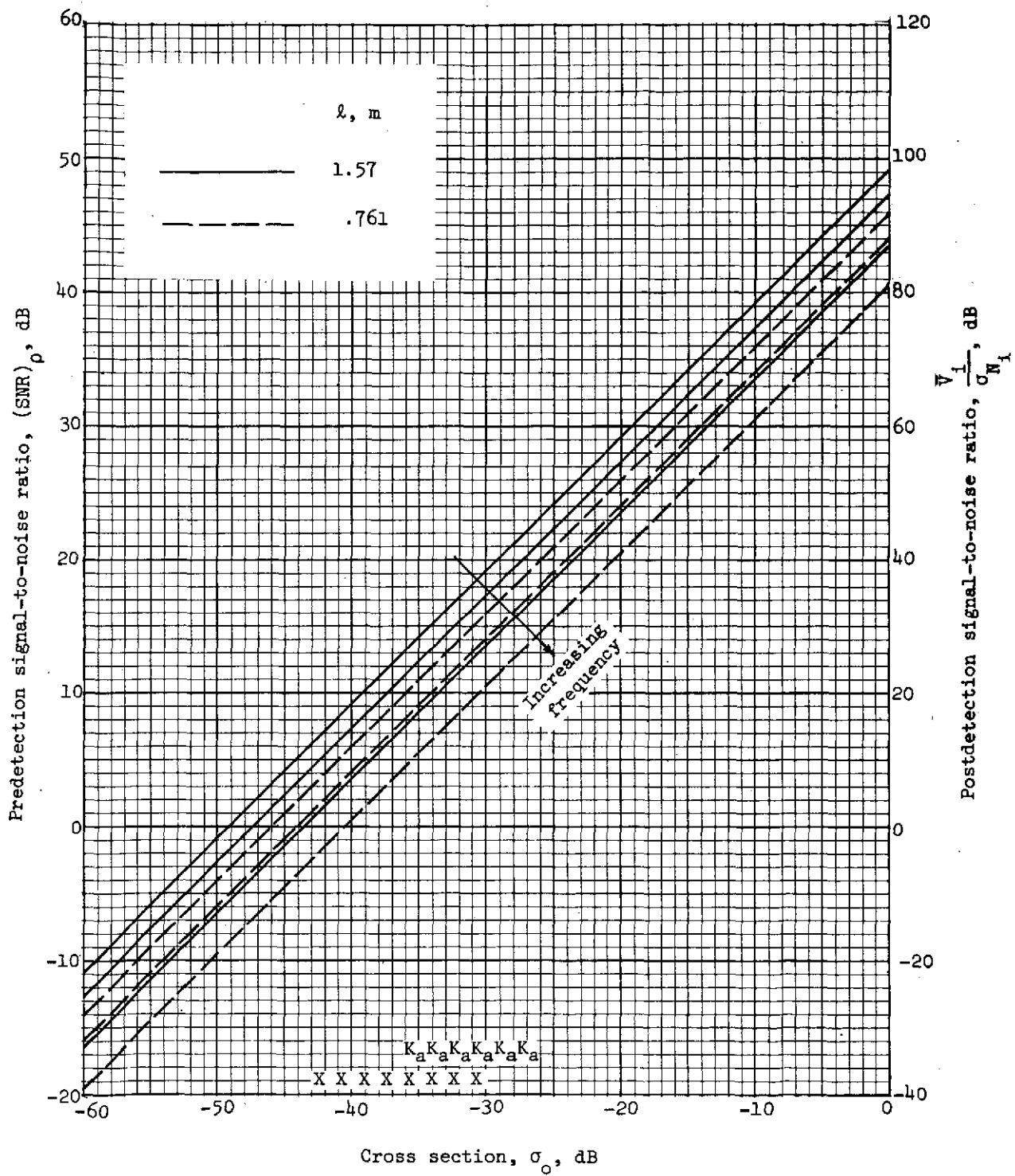
Figure 10.- SNR for constant antenna length.

Figure 11.- SNR at R = 6 km for 10, 15, and 35 GHz.

where a and b are constants. Equation (25) corresponds to equation (6-88) in reference 10, where the constant c has been set equal to zero. From equation (6-92) of reference 10, the square of the average (dc) detector output current with a signal-plus-noise input is given by

$$I_{DC}^2 = a^2 \left[\sigma^2 + \left(A_c^2/2 \right) \right]^2 \tag{26}$$

where A_c is the peak carriage voltage and σ is the root-mean-square noise voltage. Similarly, from Panter's equation (6-95) the average fluctuating (ac) output current squared with noise only at the input is given by

$$\overline{I_{AC}^2} = a^2 \sigma^4 \tag{27}$$

Taking the ratio of equations (26) and (27), the output power signal-to-noise ratio is

$$\frac{I_{DC}^2}{\overline{I_{AC}^2}} = \frac{\left[\sigma^2 + \left(A_c^2/2 \right) \right]^2}{\sigma^4} \tag{28}$$

In the notation of this report, equation (28) becomes

$$\frac{\overline{V_i}^2}{\sigma_{N,i}^2} = \frac{\left[kTF\left(1/\tau_p\right) + P_R \right]^2}{\left[kTF\left(1/\tau_p\right) \right]^2} = \left[(SNR)_\rho + 1 \right]^2 \approx (SNR)_\rho^2 \quad \text{for} \quad (SNR)_\rho \gg 1 \tag{29}$$

In figure 11 note that the actual postdetection SNR at low input (predetection) SNR's departs somewhat from the linear (in dB) relationship shown. However, these low input SNR's, say below 0 dB, are not adequate for the radar imaging ILM, so this departure will be neglected. The approximate ranges of values for the cross section of grassy targets are shown along the abscissa of figure 11 by X's and K_a's for 10 GHz and 35 GHz, respectively.

Pulse integration.- The signal-to-noise ratio in equation (19), and in figures 9, 10, and 11, is the ratio of the mean signal power received from the backscatter of one pulse from a resolution element to the root-mean-square noise power in the IF bandwidth. The received signal is the vector sum of the return from many random scatters and is a fluctuating signal. The signal voltage in the IF section can be written as

$$S(t) = V(t) \cos \left[\omega t + \theta(t) \right] \tag{30}$$

The envelope $V(t)$ is a nonstationary random process described by Rayleigh statistics. Similarly, the phase $\theta(t)$ is a uniformly distributed random process. Now at a fixed range and with a fixed target the processes are stationary. Let

26

$$P = \frac{V_i^2}{2} \tag{31}$$

Then P, a random variable denoting the received power, is exponentially distributed with probability density function

$$f(P) = \begin{cases} \dfrac{1}{P_R} e^{-P/P_R} & (P \geqq 0) \\ \\ 0 & (P < 0) \end{cases} \tag{32}$$

The mean value of P is found as follows:

$$E\{P\} = \overline{P} = \int_0^\infty P\, f(P)dP = P_R \tag{33}$$

Thus the mean value of the received signal power is P_R as calculated from the radar equation (eq. (9)).

In a similar manner the standard deviation of the received power is found to be

$$\sigma_P = P_R = \overline{P} \tag{34}$$

It is well known that the envelope of narrow band Gaussian noise also obeys Rayleigh statistics. Therefore, the signal and the noise in the ILM receiver have both a fluctuating, or ac, component and a constant, or dc, component. If a square law detector is used, the ratio at the detector output of the dc component to the ac component is

$$\frac{\overline{V_i}}{\sigma_{V,i}} = \frac{P_R}{P_R} = 1 \tag{35}$$

This ac component, or target clutter, produces a noise, sometimes called salt and pepper, in the image and affects the image quality much like receiver noise.

Depending on the antenna beamwidth and scan rate and on the pulse repetition frequency, more than one pulse may be reflected from a resolution element during a scan. If so, these pulses may be added in the receiver to improve the signal-to-noise ratio. If the azimuthal beamwidth is θ_c, the scan rate s, the scan width ϕ_L, and the pulse repetition frequency p, then N_R, the number of pulses received during the time the antenna is scanning an angular distance of one beamwidth, is

$$N_R = \frac{\theta_c p}{\phi_L s} \tag{36}$$

In order that the resolution be limited by the antenna and not by the sampling process, assume that two samples per beamwidth (after integration) are required. Then N_I, the number of pulses that can be integrated, is

$$N_I = \frac{\theta_c p}{2\phi_L s} \tag{37}$$

Using equation (37), N_I is plotted in figure 12 as a function of θ_c for several values of the ratio p/s and $\phi_L = 30^{\circ}$. Likewise, the time per sample, t_I, that is, the time required to scan an angle $\theta_c/2$, is

$$t_I = \frac{\theta_c}{2\phi_L s} \tag{38}$$

In figure 13, t_I is plotted as a function of θ_c for $\phi_L = 30^{\circ}$ and several values of s.

The integration time is also limited by another factor. In order that the along-track · resolution be limited by the pulse width, the integration time must not exceed the time required for the aircraft to travel a small fraction, say $1/10$, of the along-track resolution. This maximum integration time $t_{I,max}$ is computed as follows:

$$\left. \begin{aligned} vt_{I,max} &= \frac{\rho_a}{10} = \frac{c\tau_p}{20} \\[2mm] t_{I,max} &= \frac{c\tau_p}{20v} \end{aligned} \right\} \tag{39}$$

Using equation (39), $t_{I,max}$ is plotted in figure 14 as a function of aircraft velocity v.

Let V be the signal voltage and N be the noise voltage after square-law detection and integration (summation) in the digital processor. Then

$$V = \sum_{i=1}^{N_I} V_i \tag{40}$$

Then the mean value of V is

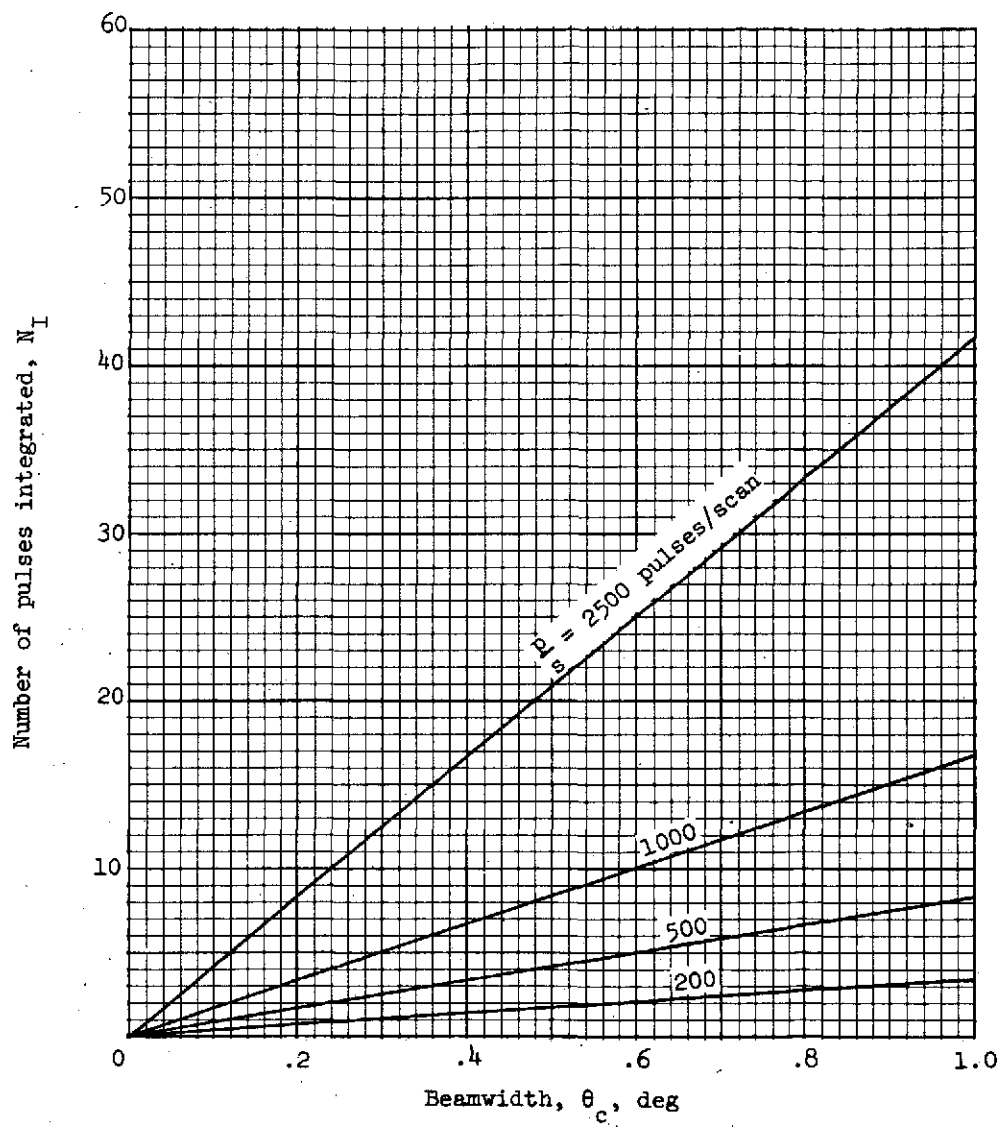$$\overline{V} = E\left\{ \sum_{i=1}^{N_I} V_i \right\} = N_I \overline{V}_i \tag{41}$$
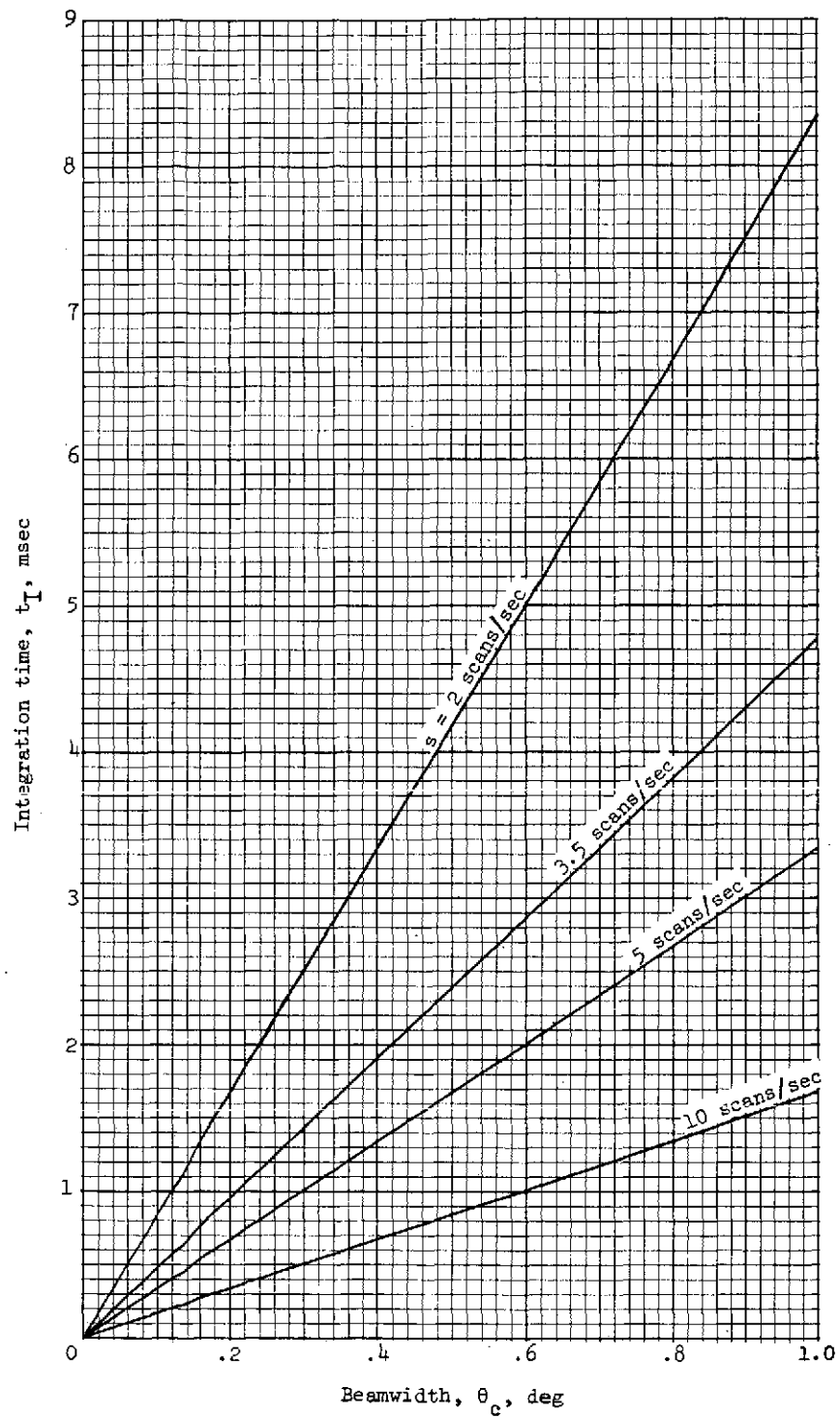
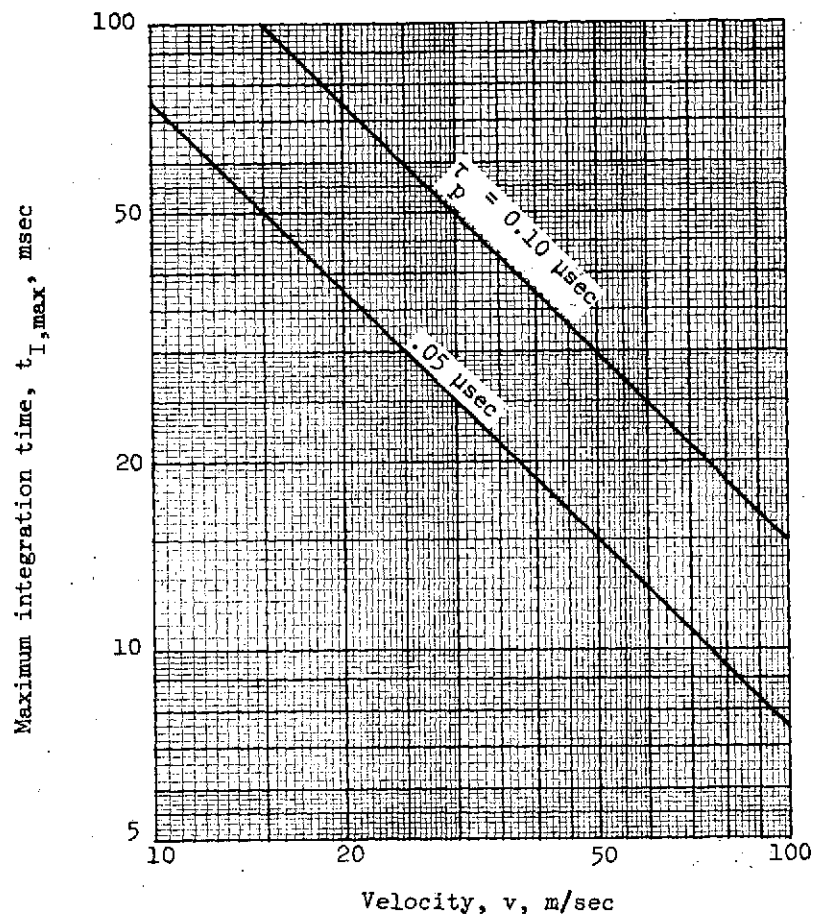Figure 12.- Number of pulses integrated.

Figure 13.- Integration time.

Figure 14.- Maximum integration time.

The mean noise voltage is likewise

$$\overline{N} = E\left\{\sum_{i=1}^{N_I} N_i\right\} = N_I\overline{N}_i \tag{42}$$

The noise has a variance given by

$$\sigma_N^2 = \overline{N^2} - \overline{N}^2$$

$$= E\left\{\left(\sum_{i=1}^{N_I} N_i\right)^2\right\} - \overline{N}^2$$

$$= E\left\{\sum_{i=1}^{N_I} N_i^2 + \sum_{i=1}^{N_I} \sum_{\substack{j=1 \\ j\neq i}}^{N_I} N_i N_j\right\} - \overline{N}^2$$

$$= N_I E\left\{N_i^2\right\} + N_I(N_I - 1) E\left\{N_i N_j\right\} - \overline{N}^2 \tag{43a}$$

Since the noise during adjacent pulses is uncorrelated, equation (43a) becomes

$$\sigma_N^2 = N_I\overline{N_i^2} + N_I^2\overline{N_i^2} - N_I\overline{N_i^2} - \overline{N}^2$$

$$= N_I\left(\overline{N_i^2} - \overline{N_i}^2\right)$$

$$= N_I\sigma_{N,i}^2 \tag{43b}$$

or

$$\sigma_N = \sqrt{N_I}\sigma_{N,i}$$

As a result, the signal-to-noise ratio (dc-signal/ac-noise) becomes after integration

$$\frac{\overline{V}}{\sigma_N} = \frac{N_I\overline{V}_i}{\sqrt{N_I}\sigma_{N,i}} = \sqrt{N_I}\frac{\overline{V}_i}{\sigma_{N,i}} \tag{44}$$

which is an improvement by the factor $\sqrt{N_I}$. This factor is shown graphically in figure 15.
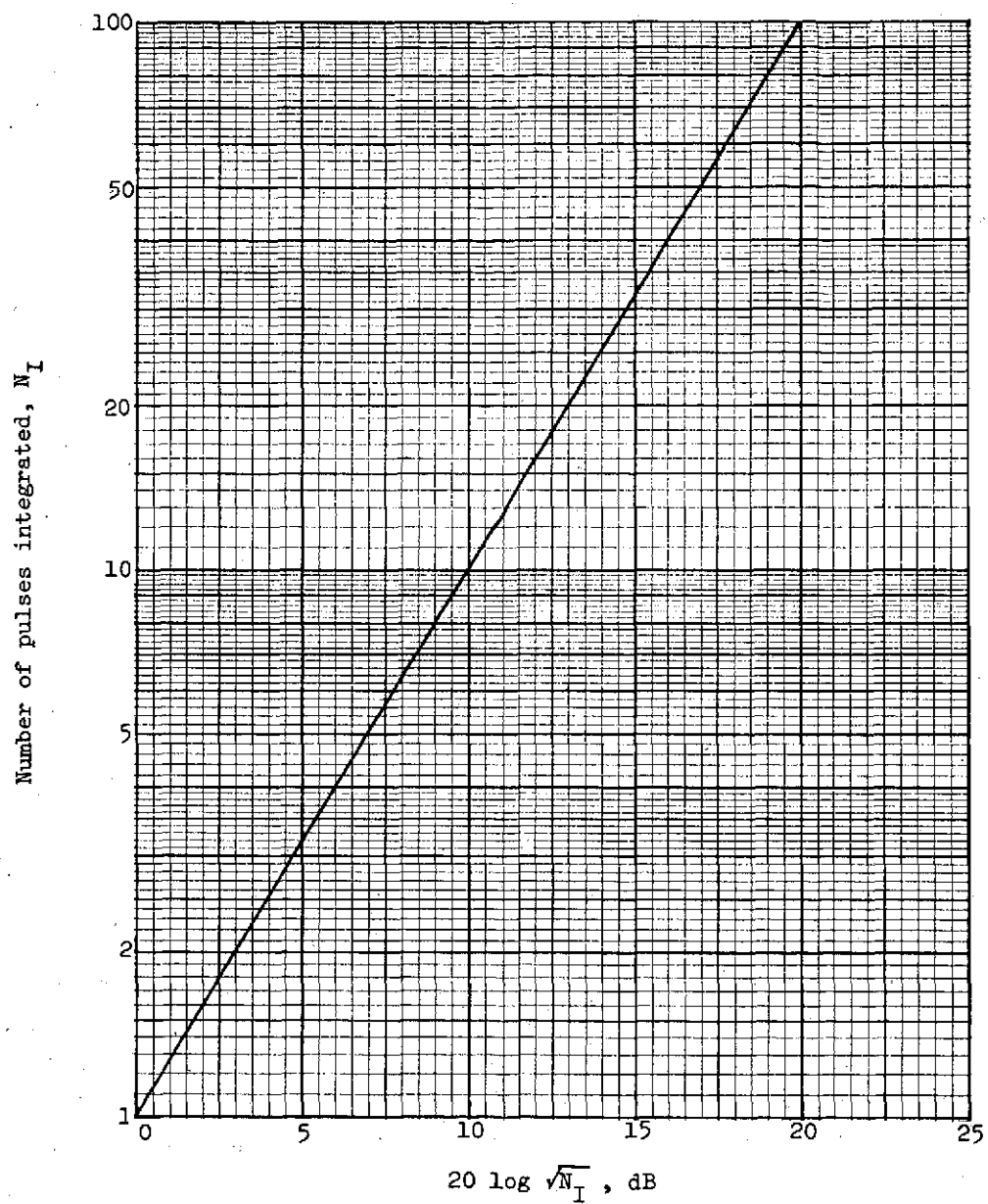
32

Figure 15.- Integration improvement factor.

Consider now the situation in which the baseline ILM is operating at a range of 6 km with an antenna length of either 0.761 m (30 in.) or 1.57 m. The single pulse signal-to-noise ratio for this situation has been plotted in figure 11. The antenna beamwidths for this case can be obtained from equation (5) and figure 4 and are tabulated in table IV. For a scan rate of 5 scans/sec, an azimuthal field of view of 30°, and a pulse repetition frequency of 5000 pulses/sec the number of pulses integrated, integration time, and integration improvement factor are calculated from equations (37), (38), and (44), respectively, and are tabulated in table IV. Addition of the integration improvement factor to the single pulse signal-to-noise ratio from figure 11 produces the postintegration signal-to-noise ratio as plotted in figure 16.

TABLE IV.- INTEGRATION IMPROVEMENT

Parameter	ℓ = 0.761 m (30 in.)			ℓ = 1.57 m		
	10 GHz	15 GHz	35 GHz	10 GHz	15 GHz	35 GHz
θ_c, deg	2.26	1.50	0.645	1.09	0.730	0.313
N_I	37.7	25.0	10.7	18.2	12.2	5.2
$20 \log \sqrt{N_I}$, dB	15.8	14.0	10.3	12.6	10.9	7.2
t_I, msec	15.1	10.0	4.3	7.3	4.9	2.1
τ_{90}, msec	14.8	9.9	4.2	14.8	9.9	4.2
$t_{I,max}$, msec	20.8	20.8	20.8	20.8	20.8	20.8

Pulse-to-pulse correlation: In order to compute the signal-to-clutter ratio $\overline{V}/\sigma_V$, after integration, the autocorrelation function of the return signal must first be determined. Consider a resolution element ρ at a range R and centered at coordinates x,y as in figure 17. To determine the autocorrelation function, first determine the doppler power spectral density of the return from ρ. For a small resolution element, the variations of σ_o and path loss over the element are negligible, and the average backscatter power is uniform over ρ. For a CW (continuous-wave) transmitted signal, the doppler spectral density is rectangular and is centered about the mean doppler frequency f_d. Find f_d as follows:

$$R = \sqrt{h^2 + x^2 + y^2} \tag{45}$$

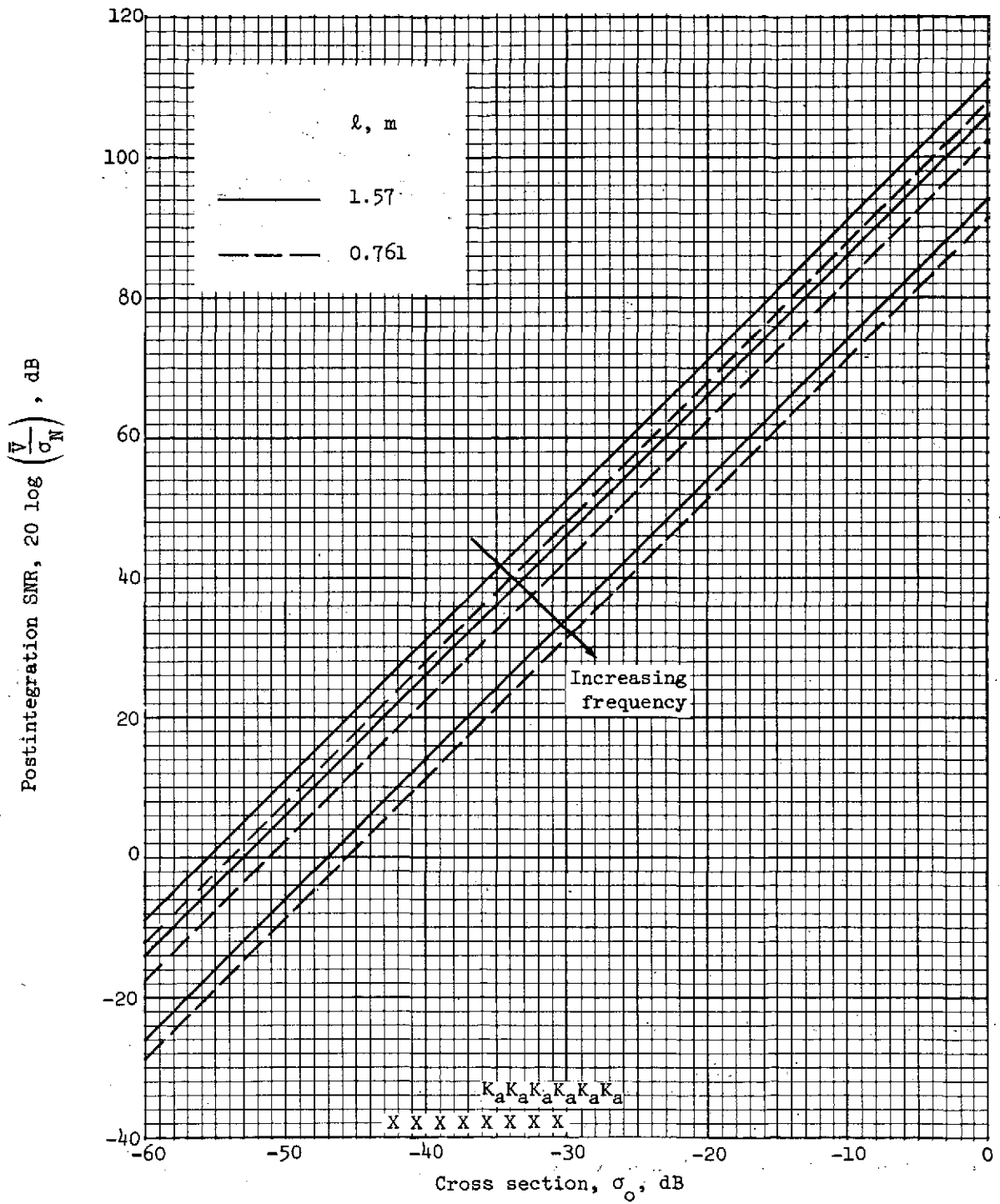$$\dot{R} = \frac{h}{R} \dot{h} + \frac{x}{R} \dot{x} + \frac{y}{R} \dot{y} \tag{46a}$$
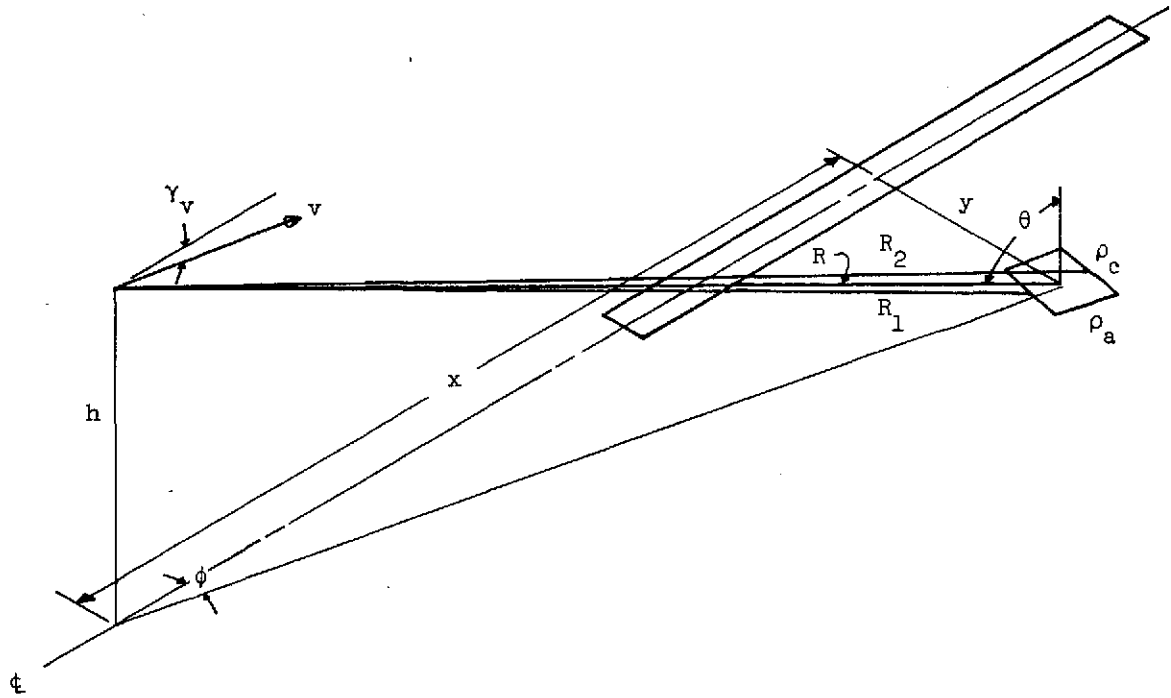
Figure 16.- Postintegration SNR at R = 6 km.

Figure 17.- Geometry for determining correlation.

$$\dot{h} = -v \sin \gamma_v \qquad (46b)$$

$$\dot{x} = -v \cos \gamma_v \qquad (46c)$$

$$\dot{y} = 0 \qquad (46d)$$

Substitution of equations (46b) to (46d) into equation (46a) produces

$$\dot{R} = -\frac{hv \sin \gamma_v + xv \cos \gamma_v}{R} \qquad (47)$$

The mean doppler frequency is then

$$f_d = -\frac{2\dot{R}f_c}{c} = \frac{2f_c v}{cR}\left(h \sin \gamma_v + x \cos \gamma_v\right) \qquad (48)$$

For a glide slope γ_v of approximately 3°

$$\sin \gamma_v \approx 0 \qquad (49a)$$

$$\cos \gamma_v \approx 1 \qquad (49b)$$

Then f_d is approximately

$$f_d \approx \frac{2f_c v x}{cR} \tag{50}$$

The limits of the rectangular spectrum can be found approximately from the rate of change of the ranges R_1 and R_2 (see fig. 17):

$$R_1 \approx \sqrt{h^2 + \left(x - \frac{\rho_a}{2}\right)^2 + y^2} \tag{51}$$

$$\dot{R}_1 \approx -\frac{\left(x - \frac{\rho_a}{2}\right)v}{R} \tag{52}$$

The lower limit of the doppler is then

$$f_1 = \frac{2\left(x - \frac{\rho_a}{2}\right)v f_c}{cR} \tag{53}$$

Similarly, the upper limit is

$$f_2 = \frac{2\left(x + \frac{\rho_a}{2}\right)v f_c}{cR} \tag{54}$$

Substituting from equation (3) for ρ_a, equations (53) and (54) become

$$\left.\begin{array}{l} f_1 = \dfrac{2\left(x - \dfrac{c\tau_p}{4}\right)v f_c}{cR} \\[3em] f_2 = \dfrac{2\left(x + \dfrac{c\tau_p}{4}\right)v f_c}{cR} \end{array}\right\} \tag{55}$$

and the doppler bandwidth Δf is

$$\Delta f = f_2 - f_1 = \frac{v f_c \tau_p}{R} \tag{56}$$

Let

$$\left. \begin{array}{l} \omega_d = 2\pi f_d \\ \omega_c = 2\pi f_c \\ \Omega = \pi \Delta f \end{array} \right\}$$ (57)

The normalized predetection spectrum $S_{pp}(\omega)$ is shown in figure 18(a).

After square-law detection, the doppler power spectral density $S_{dd}(\omega)$ can be obtained by convolution as follows:

$$S_{dd}(\omega) = S_{pp}(\omega) * S_{pp}(\omega) = \int_{-\infty}^{\infty} S_{pp}(\omega - \omega')S_{pp}(\omega')d\omega'$$ (58)

The postdetection spectrum is shown in figure 18(b), where $S_{vv}(\omega)$ is the spectrum after low-pass filtering.

The autocorrelation function $R_{vv}(\tau)$ of the detected signal can now be obtained by taking the Fourier transform of the spectral density

$$R_{vv}(\tau) = \int_{-\infty}^{\infty} S_{vv}(\omega)e^{j\tau\omega} d\omega$$

$$= \int_{-2\Omega}^{0} \left(\frac{\omega + 2\Omega}{2\Omega}\right)e^{j\tau\omega} d\omega + \int_{0}^{2\Omega} \left(\frac{2\Omega - \omega}{2\Omega}\right)e^{j\tau\omega} d\omega$$

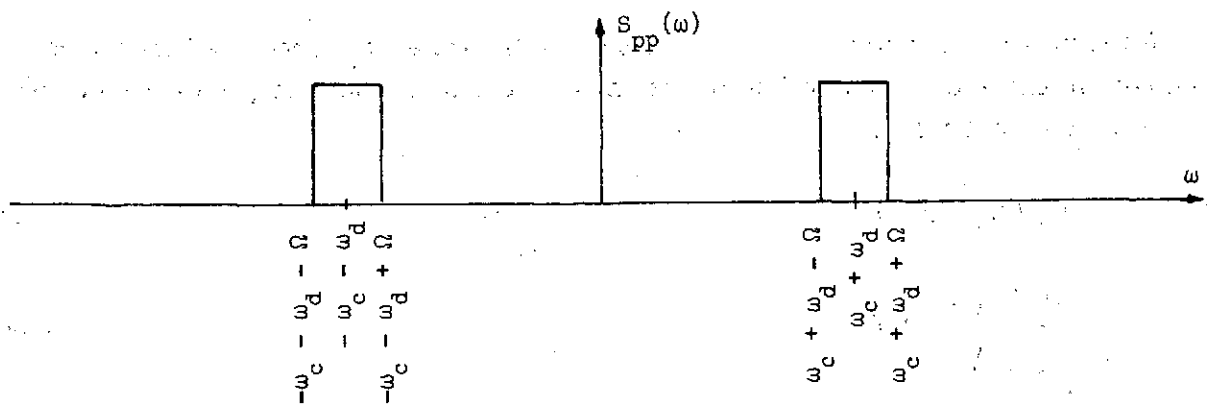$$\simeq \frac{2 \sin^2 \Omega\tau}{\left(\Omega\tau\right)^2}$$ (59)

The correlation coefficient is then

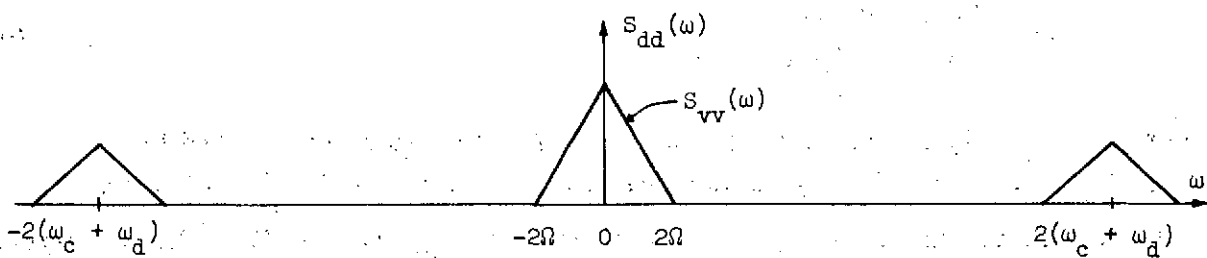$$\rho_{vv}(\tau) = \frac{R_{vv}(\tau)}{R_{vv}(0)} = \frac{\sin^2 \Omega\tau}{(\Omega\tau)^2}$$ (60)

which is shown graphically in figure 19. Substitution for Ω from equations (57) and (56) produces

$$\rho_{vv}(\tau) = \frac{\sin^2\left(\dfrac{\pi v f_c \tau_p \tau}{R}\right)}{\left(\dfrac{\pi v f_c \tau_p \tau}{R}\right)^2}$$ (61)

Equation (61) is also plotted in figure 19 for $v = 72$ m/sec, $R = 6$ km, $\tau_p = 0.1$ μsec, and $f_c = 35$ GHz.

38

(a) Predetection.

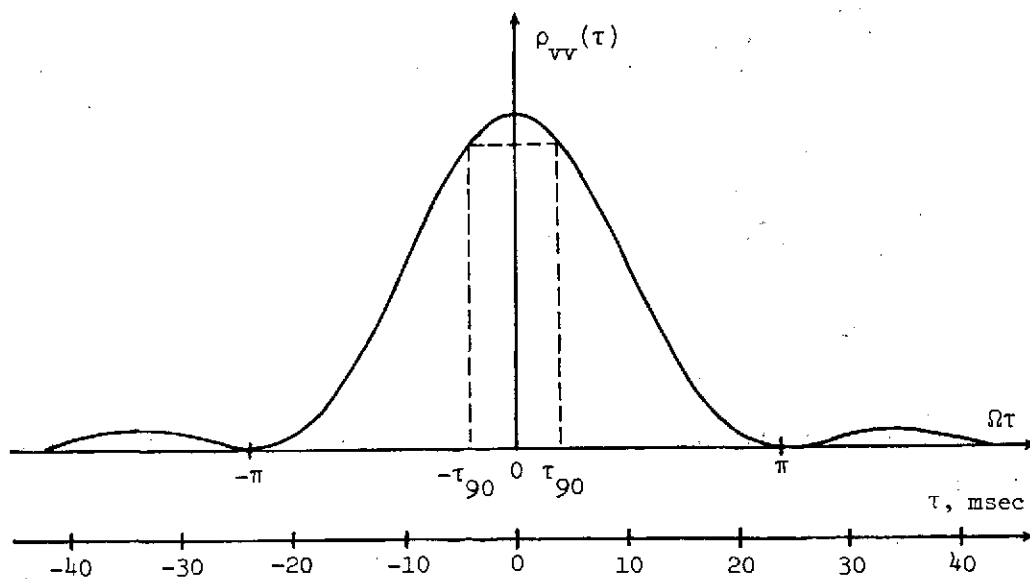(b) Postdetection.

Figure 18.- Doppler power spectral density.

Figure 19.- Correlation coefficient for general case and for specific case of R = 6 km,
$\tau_p = 0.1 \,\mu sec$, $f_c = 35$ GHz.

If the pulse integration time t_I is less than the time τ_{90} required for the correlation coefficient to decrease to 0.9, then to a good approximation the pulses can be considered to be completely correlated. Let

$$\rho_{vv}\left(\tau_{90}\right) = 0.9 \tag{62a}$$

$$\frac{\sin^2 \Omega \tau_{90}}{\left(\Omega \tau_{90}\right)^2} = 0.9 \tag{62b}$$

$$\Omega \tau_{90} = 0.559 \tag{62c}$$

$$\tau_{90} = \frac{0.559}{\Omega} = \frac{0.559R}{\pi v f_c \tau_p} \tag{62d}$$

In figure 20, τ_{90} is plotted as a function of R for two values of τ_p and for $v = 72$ m/sec. In table IV, τ_{90} is tabulated for $R = 6$ km and $\tau_p = 0.1$ μsec.

Clutter reduction: By comparing the values for τ_{90} in table IV to the corresponding values for t_I, it can be seen that the pulse return is essentially correlated over the integration interval for the baseline ILM operating at a range of 6 km. In this case the variance σ_V^2 of the signal (ac component) after integration of N_I pulses is

$$\sigma_V^2 = \overline{V^2} - \overline{V}^2$$

$$= E\left\{\left(\sum_{i=1}^{N_I} V_i\right)^2\right\} - \overline{V}^2$$

$$= N_I^2 \overline{V_i^2} - N_I^2 \overline{V_i}^2$$

$$= N_I^2 \sigma_{V,i}^2 \tag{63}$$

Combining equations (63), (41), and (35) the ratio of signal to target clutter, after integration, is found to be

$$\frac{\overline{V}}{\sigma_V} = \frac{N_I \overline{V_i}}{N_I \sigma_{V,i}} = 1 \tag{64}$$

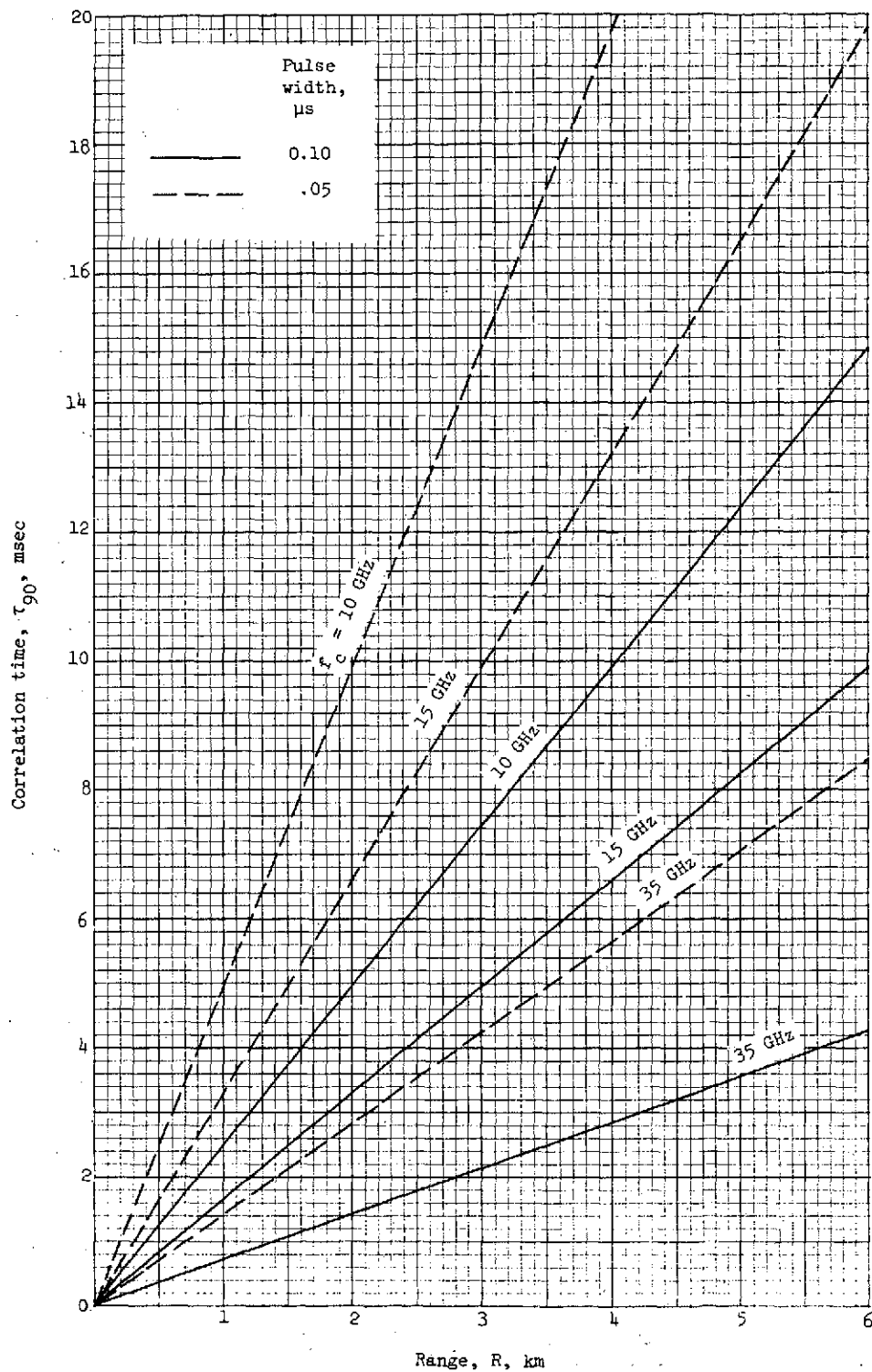and there is no improvement in the signal-to-clutter ratio $(SCR)_T$ by integration.

Figure 20.- Correlation time τ_{90} for $v = 72$ m/sec.

From equation (62d) or figure 20, it can be seen that τ_{90} is a function of range. At ranges less than 6 km the pulses decorrelate more quickly, and there may be a slight improvement in the signal-to-clutter ratio by integration.

If clutter reduction by integration is required, it can be accomplished by changing the frequency from pulse to pulse.

Required signal-to-noise ratio.- In order to use the information presented in the preceeding sections to complete the system design of an ILM imaging radar, it is necessary to know the signal-to-noise ratio required to produce an acceptable image. A considerable amount of information concerning the effects of random noise on television and other image-type displays has been published in the literature, including references 11 to 16. References 14 and 16 indicate that the SNR required for detection of a rectangular target or a bar chart is a function of the target size and is less than unity. Reference 15 indicates that previous studies determined the SNR requirements for detection to be 6.7 and 7. However, these SNR's are not defined and hence cannot be used. Levine, Jauer, and Kozlowski (ref. 15) found that detection performance increased monotonically with increasing SNR up to SNR = 100, the highest in their experiment. They defined SNR as the ratio of video rms voltage to random noise rms voltage (at the television monitor input). Since the target and background are unknown in this case, it is difficult to apply their results to the radar imaging ILM problem. Reference 12 presents the results of a subjective test of the effects of random noise and cochannel interference on commercial type television. The noisy pictures were given ratings of unusable, inferior, marginal, passable, fine, and excellent by each of 92 observers. Ratings of inferior and marginal are defined in reference 17 as follows: Inferior — "The picture is very poor but you could watch it. Definitely objectionable interference is present." Marginal — "The picture is poor in quality and you wish you could improve it. Interference is somewhat objectionable." In reference 12 the pictures with a signal-to-noise ratio of approximately 23 dB were given a rating of marginal or better by 50 percent of the observers and a rating of inferior or better by 95 percent of the viewers. Furthermore, images with an SNR of about 17 dB were rated inferior or better by 50 percent of the observers. In this study (ref. 12) the signal amplitude used in the SNR calculations was measured during the sync pulses. Therefore, the SNR of the image would be less than the numbers quoted above.

The required signal-to-noise ratio for the radar imaging ILM cannot be accurately concluded. However, based on the referenced studies, a required postintegration SNR of 15 dB will be assumed.

Required signal-to-clutter ratio $(SCR)_T$.- Similarly, the performance of an ILM imaging radar cannot be fully evaluated without a knowledge of the required signal-to-target clutter ratio $(SCR)_T$. Both theoretical and experimental work has been done on techniques for reducing clutter in radar images. (See, e.g., refs. 18 to 20.) However,

neither of these studies specifies the $(SCR)_T$ required nor do they present images at different specified $(SCR)_T$'s for evaluation. It must be stated then that the requirements on signal-to-clutter ratio are undetermined, and further work in this area must be done.

Results for area targets.- From the foregoing analysis, the following results are obtained for area targets:

1. At a range of 6 km and with a 2 m antenna length, an imaging radar ILM operating at a frequency of 35 GHz will have a cross-track resolution of 25.7 m (84.3 ft), which nearly satisfies the resolution requirement of 23 m (75 ft) and is sufficient to produce an image of a 45.7 m (150 ft) runway. The resolution with a 1.57 m antenna at the same frequency is 32.8 m (108 ft) and does not quite satisfy the requirement but may be adequate. The resolutions at 35 GHz with a 0.761 m (30 in.) antenna and with any antenna lengths up to 2 m at 15 GHz and 10 GHz are at least 60 m and do not nearly meet the requirement.

2. Even if the maximum range could be reduced to 4.25 km, corresponding to the range to the far end of a 3.66 km (12 000 ft) runway from a 30.5 m (100 ft) altitude, radar imaging ILM's operating at 10 GHz or 15 GHz do not meet the 23 m resolution requirement with antenna lengths up to 2 m. If a cross-track resolution equal to the runway width (typically 45.7 m) were found to be acceptable, then a radar imager with a 2 m antenna at 15 GHz, which has a resolution of 42.5 m (139 ft), would be adequate. At 4.25 km a 35 GHz imager has cross-track resolutions of 18.2 m (59.7 ft), 23.2 m (76.1 ft), and 48.0 m (158 ft) with antenna lengths of 2m, 1.57 m, and 0.761 m (30 in.), respectively. The cross-track resolution capabilities of the radar imaging ILM are summarized in table V.

3. The differential radar cross section σ_o of the runway surroundings (grass, weeds, dirt, etc.) varies from -43 to -18 dB and from -36 to -18 dB at X-band and K_a-band, respectively, for incidence angles from 89° to 80°. The cross section of undisturbed snow is approximately -40 to -50 dB. The cross section of concrete is in the range of -46 to -63 dB at X-band and -35 to -47 dB at K_a-band.

4. From figure 10, without pulse integration the signal-to-noise ratio with baseline parameter values and a 1.57 m antenna is sufficient to produce an adequate image of a runway surrounded by grass or weeds out to 6 km. With a 0.761 m (30 in.) antenna the SNR is too low at 6 km. With either antenna the return from the concrete at 6 km is masked by noise.

5. Using postdetection pulse integration the SNR of the return from grass can be improved sufficiently to produce an adequate image (from the standpoint of SNR) at 6 km with a 0.761 m (30 in.) antenna.

6. The signal from undisturbed snow at 6 km is masked by noise even with pulse integration, assuming 5 scans/sec and 5000 pulses/sec. Even with sufficient SNR the cross sections of undisturbed snow and concrete overlap, and there may be insufficient

TABLE V.- CROSS-TRACK RESOLUTION AT RANGES

OF 6 KM AND 4.25 KM

Frequency, GHz	Range, km	Antenna length, m	Cross-track resolution		Adequacy[a]		
			m	ft	Adequate	Marginal	Inadequate
35	6.00	2.00	25.7	84.3	X		
		1.57	32.8	108		X	
		[b].761	67.8	223			X
	4.25	2.00	18.2	59.7	X		
		1.57	23.2	76.1	X		
		[b].761	48.0	158			[c]X
15	6.00	2.00	60.0	197			X
		1.57	76.2	250			X
		[b].761	158	518			X
	4.25	2.00	42.5	139			[c]X
		1.57	54.0	177			[c]X
		[b].761	112	367			X
10	6.00	2.00	90.0	295			X
		1.57	115	376			X
		[b].761	236	776			X
	4.25	2.00	63.8	209			X
		1.57	81.2	266			X
		[b].761	168				X

[a]Based on 20 m requirement.

[b]30 in.

[c]May be usable with relaxed requirements.

contrast to produce an adequate image. The use of snow removal equipment to clear the runway might change the backscatter properties of the snow surrounding the runway sufficiently to produce a usable image. Otherwise, runway enhancement must be provided.

7. The signal-to-clutter ratio $(SCR)_T$ of a single return pulse after square-law detection is 0 dB independent of range, and this ratio cannot be improved by simple integration of pulses, because adjacent pulses will be correlated with the anticipated values of pulse width, pulse repetition frequency, and aircraft velocity. Improvement in signal-to-clutter ratio can be obtained through integration if pulse-to-pulse frequency agility were used to accomplish decorrelation. However, the requirements for signal-to-clutter ratio are not known, and additional experimentation must be performed.

Discrete Targets

Discrete targets are important in the operation of an ILM from two standpoints: first is the use of runway existing lights and approach lights, corner reflectors, etc. to enhance the runway image and second is the detection of obstructions such as aircraft and vehicles on the runway.

To examine the performance of a radar imager with discrete targets, rewrite equation (19) to express the signal-to-noise ratio of the return from a target of radar cross section σ, assuming a fixed antenna length ℓ and elevation beamwidth θ_a,

$$SNR = \frac{P_t L^2 \eta^2 \ell^2 \sigma \tau_p}{4\pi R^4 \theta_a^2 kTF} \tag{65}$$

Using the baseline values, equation (65) becomes in dB

$$SNR = 233.9 + 20 \log \ell \ 10 \log \sigma + 10 \log \tau_p - 40 \log R \tag{66}$$

The predetection SNR from equation (66) is plotted in figure 21 as a function of radar cross section at a range of 6 km for a 0.1 μsec pulse.

From information presented in chapter 27 of reference 6 and in reference 21, it appears that 1 m^2 (0 dBsm) is a reasonable value for the minimum radar cross section of most metallic skinned aircraft. Referring to figure 21, the postdetection SNR of such aircraft should be at least 20 dB at 6 km, and the aircraft should be detected. Private aircraft with nonmetallic skins may not be detectable at 6 km. However, since the signal-to-noise ratio improves as R^{-4}, these aircraft should be detectable at slightly smaller ranges.

The most likely type of runway obstructions other than aircraft would probably be ground vehicles. While measured values of the radar cross section of vehicles have not
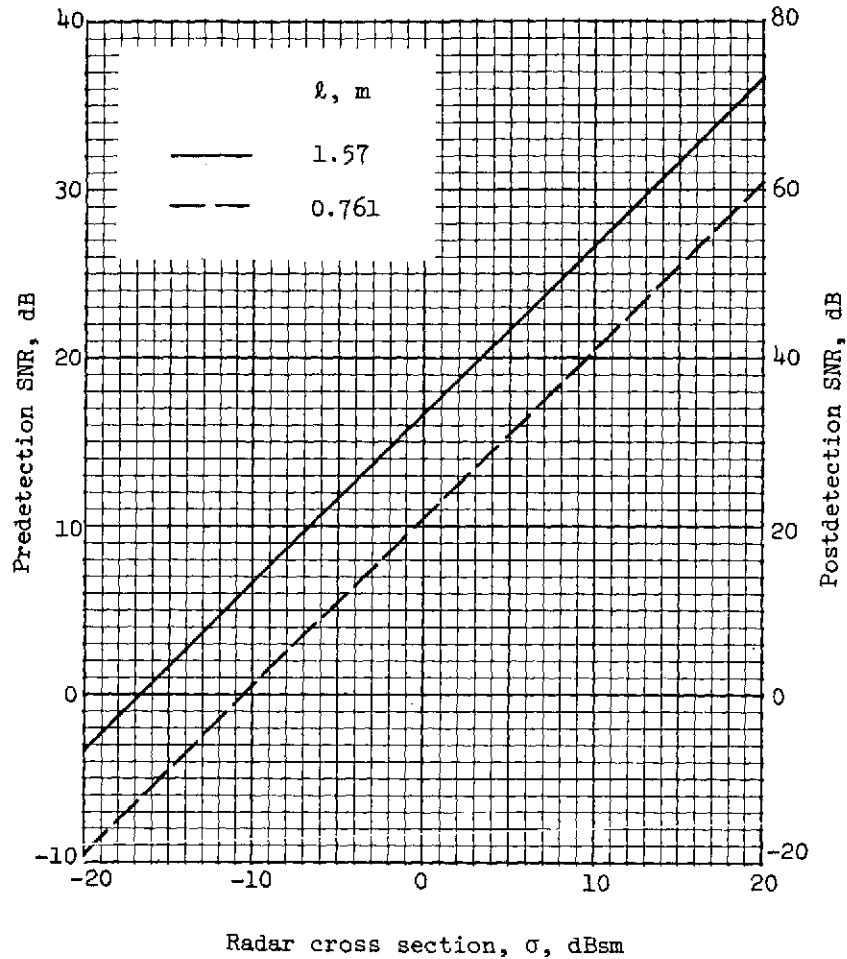
Figure 21.- SNR versus σ at R = 6 km for τ_p = 0.1 μsec.

been obtained, it seems reasonable that the cross section would be in the range of a few tenths of a square meter to a few square meters. From figure 21 it appears that the base-line system would detect many vehicles at a range of 6 km and would detect most vehicles at slightly shorter ranges. A more exact prediction of radar imaging ILM performance cannot be made with the data available.

Suppose corner reflectors are desired to enhance the edge of the runway or to mark the four corners of the runway. From Skolnik (ref. 6, ch. 27), the maximum cross section of a trihedral corner reflector is expressed by

$$\sigma = \frac{4\pi\left(0.289b^2\right)^2}{\lambda^2}$$ (67)

where b is the length of each side. From equation (67) the cross section of a 0.3048 m (12 in.) corner reflector is 10 dBsm at 10 GHz and 20.9 dBsm at 35 GHz. From figure 21, the return from such a reflector is more than sufficient for detection at 6 km.

46

WEATHER EFFECTS

- Bad weather will adversely affect the performance of a microwave radar imager in two ways: (1) reduction of received signal strength by attenuation and (2) introduction of a noiselike interference, or weather clutter, by reflection of the transmitted signal from the precipitation. The performance of the ILM in bad weather is particularly important since the ILM will be most valuable as a landing aid during conditions of low visibility. Those weather conditions to be considered are rain, snow, and fog. The effect of fallen snow on the backscatter properties of the surface has been considered in a previous section.

Rain

The propagation of microwaves through rain has received considerable attention in the literature from both a theoretical and experimental point of view. (See refs. 22 to 46.) The theoretical calculation of attenuation and reflectivity usually is accomplished by applying the Rayleigh and Mie theories of electromagnetic scattering to a spherical raindrop. The results are then summed over a measured distribution of drop sizes for a given rainfall rate. Because of the large variance in drop-size distributions and the inaccuracies in measurements of rainfall rate, it is not possible to present a single value of attenuation or reflectivity for a given rainfall rate and microwave frequency; rather, a range of values must be utilized.

Attenuation.- In figure 22 is plotted the range of values of attenuation as a function of rainfall rate as found by various researchers and reported in references 22 to 30 and 33 to 37. In instances where the reported frequency differed from the frequency of interest, the attenuation in dB/km was interpolated according to $f^{1.8}$ as suggested by Nathanson (ref. 38).

Consider now the signal-to-noise ratio of the return from a resolution element ρ. After modification to account for rain attenuation, assuming uniform rainfall along the propagation path, the predetection SNR in equation (22) for a fixed antenna length ℓ becomes

$$(SNR)_\rho = \frac{P_t L^2 \eta^2 \lambda \ell \sigma_o \tau_p^2 c \alpha^{-2R}}{8\pi R^3 \theta_a^2 kTF} \tag{68}$$

Assuming baseline values from table I and a square-law detector as before, the postintegration SNR at $R = 6$ km is in dB (from eqs. (24), (44), and (68))

$$SNR = 2\left[62.4 + 10 \log \lambda + 10 \log \ell + 10 \log \sigma_o - 2R(10 \log \alpha)\right] + 20 \log \sqrt{N_I} \tag{69}$$
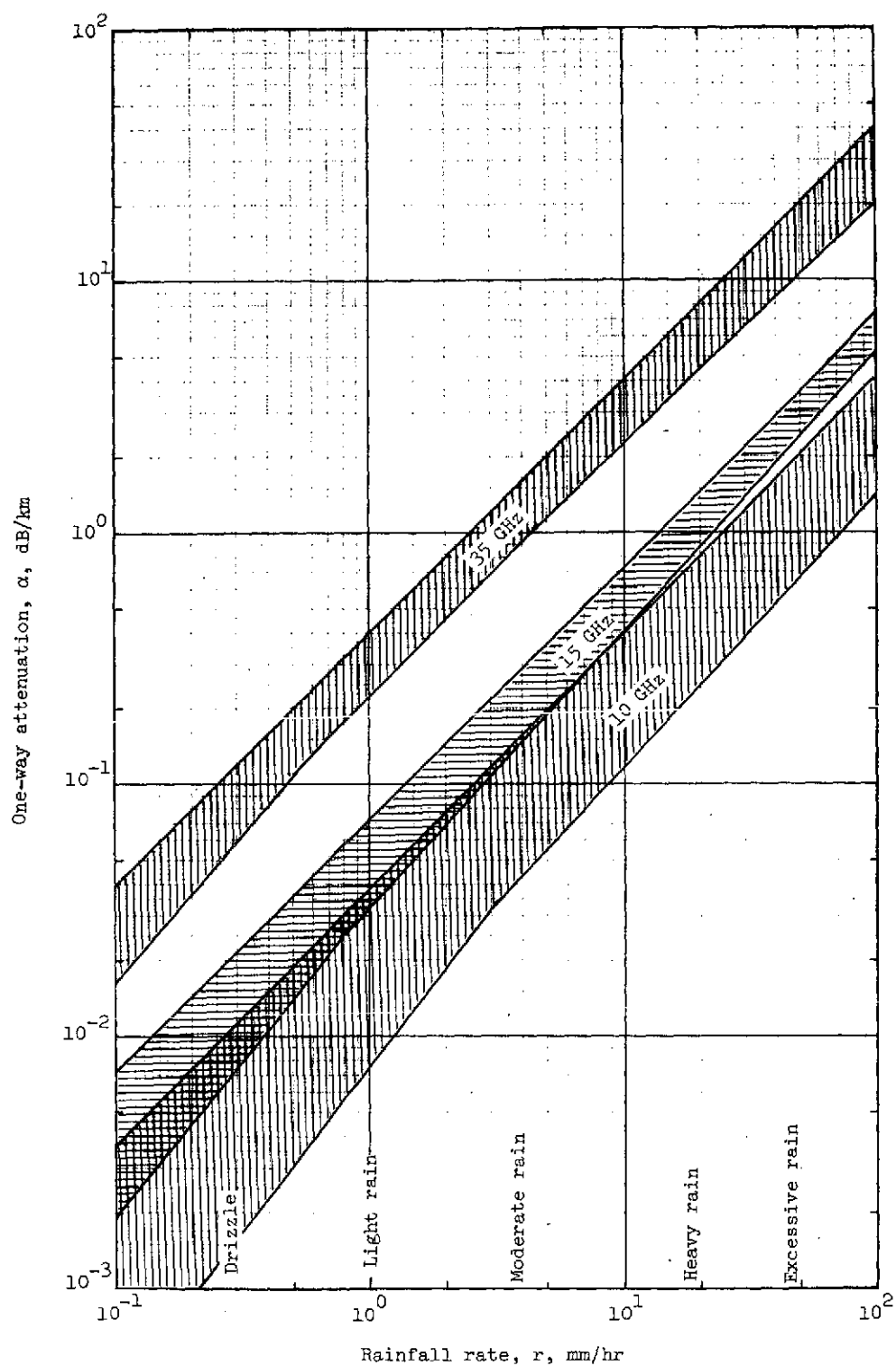
Figure 22.- Rain attenuation.

From figure 22 the attenuation factor in moderate rain (4.0 mm/hr) is between 0.043 and 0.16 dB/km at 10 GHz, between 0.15 and 0.29 dB/km at 15 GHz, and between 0.92 and 1.6 dB/km at 35 GHz. The corresponding values of two-way attenuation for a range of 6 km are 0.516 to 1.92 dB, 1.80 to 2.48 dB, and 11.0 to 19.2 dB at 10, 15, and 35 GHz, respectively. Using these values in equation (69), the post integration SNR in figure 16 has been modified to account for moderate rain and is plotted in figure 23 for an antenna length of 1.57 m.

For a threshold signal-to-noise ratio of 15 dB as before, it can be seen from figure 23 that under the given conditions the SNR from a resolution element at 6 km is inadequate in moderate rain at 35 GHz. From figure 22 the attenuation factor at 35 GHz in light rain is between 0.23 and 0.40 dB/km. The SNR for this condition is shown also in figure 23, and it is barely adequate.

Using a required SNR of 15 dB, an antenna length of 1.57 m, and the range of values of the radar cross section of weeds, grass, etc., equation (69) was used to determine the maximum attenuation limited range as a function of rainfall rate, and the results are shown graphically in figure 24. The cross-section values used to determine the tolerances, or limits, are -21 to -43 dB at 10 GHz and -18 to -36 dB at 35 GHz.

Since the uncertainty in the maximum range is so large, it would be useful to compute a nominal, or best estimate, of the maximum range. The calculations were performed using the average value for the attenuation factor α and using a best estimate of the differential radar cross section σ_o. Since grass is the most likely type of terrain bordering the runway, the σ_o of grass from table II was estimated to be -28 dB at 10 GHz and -22 dB at 35 GHz. These values were degraded by 3 dB to account for circular polarization (see the following section on rain clutter) and were degraded an additional 9 dB to account for the reduction in σ_o when going from an incidence angle of 80° to 89°.

From figure 24 it can be seen that the baseline system may be limited by attenuation at a 6 km range to a rainfall rate of 6 mm/hr at 10 GHz and only 0.4 mm/hr at 35 GHz. Consider a range of 4.25 km, which is approximately the range to the far end of a 3658 m (12 000 ft) runway from an aircraft at the 30.48 m (100 ft) decision height on a 3° glide-slope. The baseline system can operate at this range in rains of at least 21 mm/hr at 10 GHz and 1.8 mm/hr at 35 GHz.

Clutter.- Not only is the transmitted signal reflected by the target and attenuated by the precipitation, but it also is reflected by the precipitation. This reflected signal, or weather clutter, forms an interfering signal. The clutter power C returned from precipitation at a range R can be computed from the standard radar-range equation, assuming uniform rain

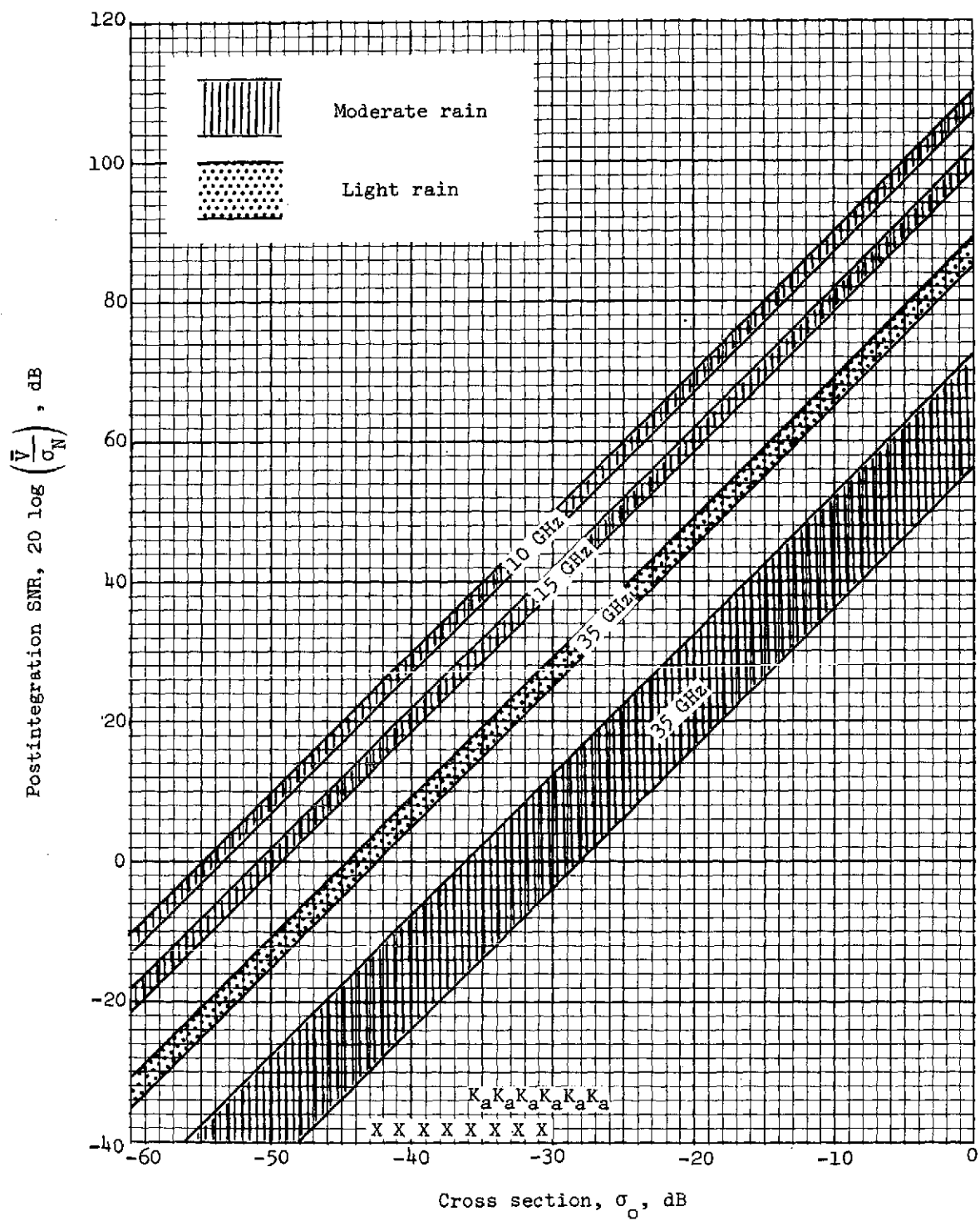$$C = \frac{P_t L^2 G A_e \sigma \alpha^{-2R}}{\left(4\pi R^2\right)^2} \tag{70}$$

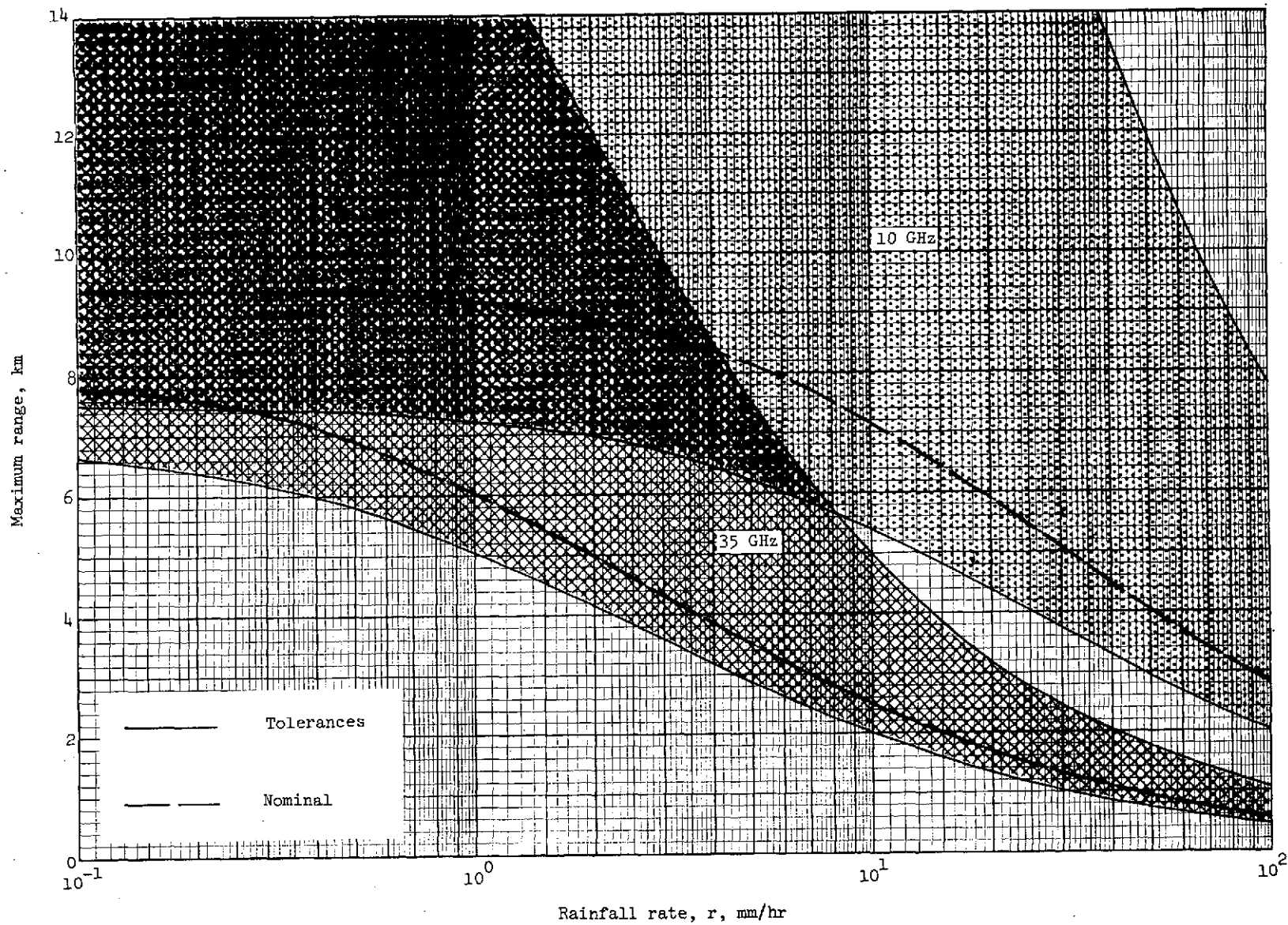Figure 23.- Postintegration SNR at R = 6 km in rain.

Figure 24.- Maximum attenuation limited range in rain.

The clutter cross section σ can be expressed as

$$\sigma = V_\rho \Sigma \tag{71}$$

where

V_ρ volume of clutter cell, m^3

Σ reflectivity of precipitation, m^2/m^3

Neglecting the effect of ground reflections, the clutter cell volume in figure 1 can be approximated by (ref. 6, pp. 24 to 29)

$$V_\rho \approx \frac{\pi R^2 \theta_a \theta_c \tau_p c}{8} \tag{72}$$

Substitution of equations (71) and (72) into equation (70) produces

$$C = \frac{P_t L^2 G A_e \theta_a \theta_c \tau_p c \Sigma \alpha^{-2R}}{128\pi R^2} \tag{73}$$

For a fixed antenna length, equation (73) becomes

$$C = \frac{P_t L^2 \eta^2 \ell \lambda c \tau_p \Sigma \alpha^{-2R}}{32 R^2 \theta_a} \tag{74}$$

From equation (68) the signal power from a resolution element under these conditions is

$$P_\rho = \frac{P_t L^2 \eta^2 \lambda \ell \sigma_o \tau_p c \alpha^{-2R}}{8\pi R^3 \theta_a^2} \tag{75}$$

From equation (74) and (75), the signal-to-clutter ratio $(SCR)_W$ is then

$$(SCR)_W = \frac{4\sigma_o}{\pi R \theta_a \Sigma} \tag{76}$$

Note from equation (76) that, unlike rain attenuation and receiver noise, the effects of weather clutter cannot be reduced by increasing transmitter power.

As previously mentioned, calculations of the radar reflectivity Σ (cross section per unit volume) or of the related effective reflectivity factor Z have been made by a

number of authors. The range of values of Σ found by Crane (ref. 33) and by Mueller and Sims (ref. 34) is plotted in figure 25 after adjustments for slight frequency differences according to f^4 as suggested by Nathanson (ref. 38). These values of reflectivity are for linearly polarized waves. To reduce the reflectivity and hence the rain clutter, circular polarization can be employed (ref. 47, ch. 17). If the rain drops were perfect spheres, if the polarization of the transmitted wave were perfectly circular, and if there were no ground reflections, then the received return from the rain would be zero because the rain reflected wave would be perfectly circularly polarized with sense opposite that of the antenna. In practice, neither of these conditions is satisfied. Measurements and calculations of the reduction in reflectivity, or clutter power, with circular polarization have been reported by several authors, and their results are tabulated in table VI. A considerable spread in the cancellation ratio is evident in the data in table V and, furthermore, the cancellation ratio may be reduced by the effect of ground reflections. This effect has been analyzed to some extent in references 41 and 42, wherein limits on the cancellation ratio of as low as 20 dB have been reported. From these sources of information it is estimated that the use of circular polarization can reduce the radar cross section of rain by 20 to 30 dB at X-band and 17 to 25 dB at K_a-band. Application of these reductions to the cross-sections in figure 24 produces the estimated reflectivities for rain for circular polarization plotted in figure 26.

The signal-to-clutter $(SCR)_W$ ratio has been calculated using equation (76) for a range of 6 km in moderate rain (4 mm/hr). From figure 26 the reflectivity Σ at this rainfall rate is between -79 and -93 dB/m at 10 GHz and between -55 and -65 dB/m at 35 GHz. The resulting $(SCR)_W$ is shown graphically in figure 27. If it is assumed that the required signal-to-clutter ratio is the same as the required signal-to-noise ratio, that is, 7.5 dB before detection and 15 dB postdetection, then figure 27 shows that the $(SCR)_W$ in moderate rain at 6 km is barely adequate at 10 GHz and inadequate at 35 GHz. Even in drizzle the $(SCR)_W$ is marginal or worse at 35 GHz.

Assuming a threshold $(SCR)_W$ of 7.5 dB, the maximum clutter limited range has been calculated from equation (76). The results are plotted in figure 28 as a function of rainfall rate. The nominal values were computed using a straight-line estimate for reflectivity in figure 26 and using the same values for σ_0 as in figure 24. Even in the nominal case the radar imaging ILM can operate at 6 km in rain of only 0.35 mm/hr or less at 35 GHz. The nominal attenuation limited range in such rain is 7.3 km, so the baseline system at 35 GHz is clutter limited.

Rainfall occurrence.- Figures 23 to 24 and 27 to 28 can be used to evaluate the performance of the ILM in terms of rainfall rate. To assist the reader in translating this information into probability of loss of data from the ILM, figure 29 provides the probability of occurrence of rainfall rate for several locations in the United States and England.
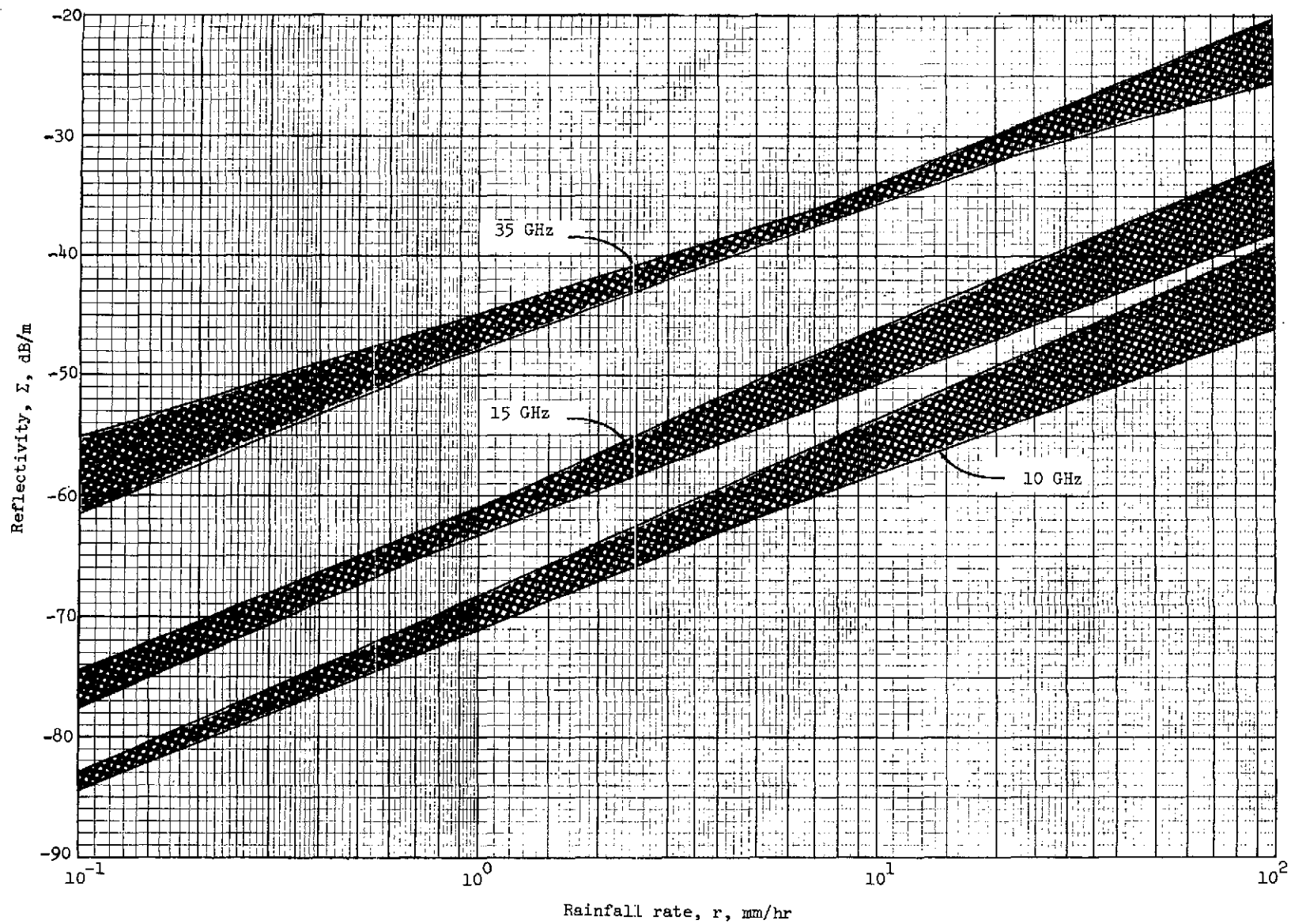
Figure 25.- Reflectivity of rain with linear polarization.

TABLE VI.- REDUCTION IN PRECIPITATION REFLECTIVITY

BY CIRCULAR POLARIZATION AS REPORTED

BY SEVERAL AUTHORS

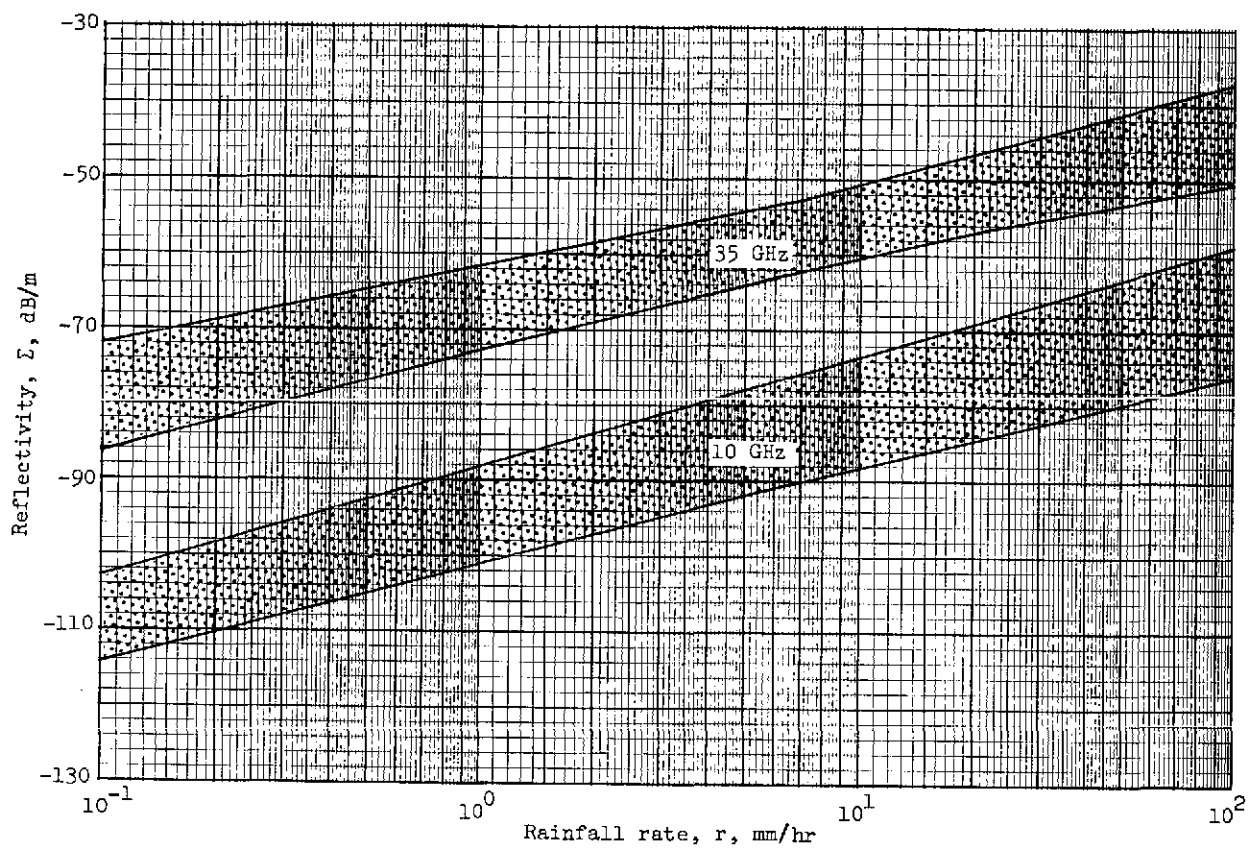| Type of precipitation	Reduction in reflectivity, dB			Reference
	X-band	K_a-band	Unspecified frequency	
Rain	28 to 30	17		39
Rain	26 to 28	17 to 18		38
Rain	12 to 19			40
Rain, 1 mm/hr			37	41
Rain, 4 mm/hr			23	41
Rain, 15 mm/hr			18	41
Thunderstorm	15			38
Dry snow		12 to 16		39
Dry snow		12 to 16		38
Fine snow	26			38
Snow	13 to 19			40
Hail	10 to 18			40
Fog			>37	41

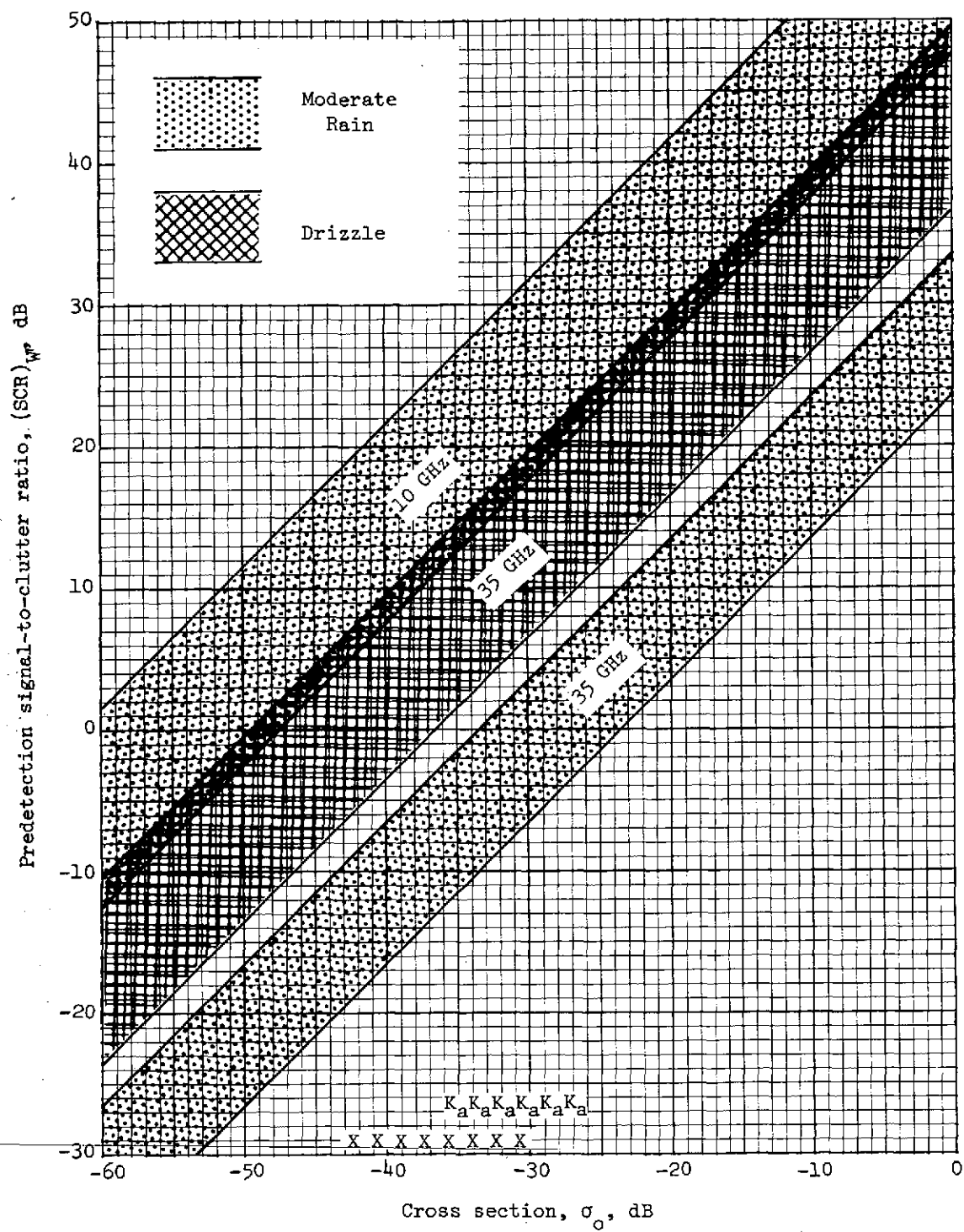Figure 26.- Reflectivity of rain with circular polarization.

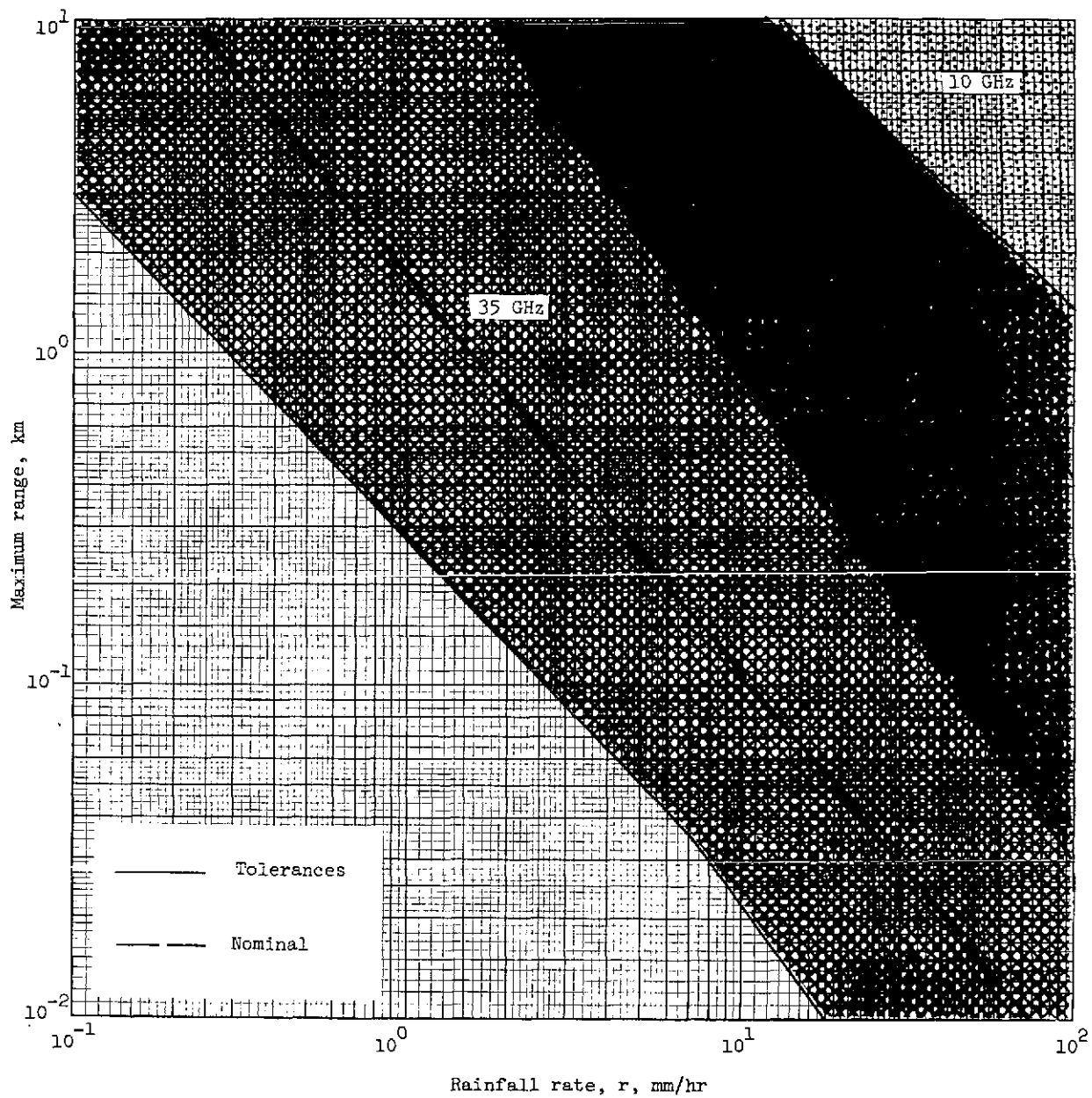Figure 27.- Predetection signal-to-clutter ratio at $R = 6$ km in rain.

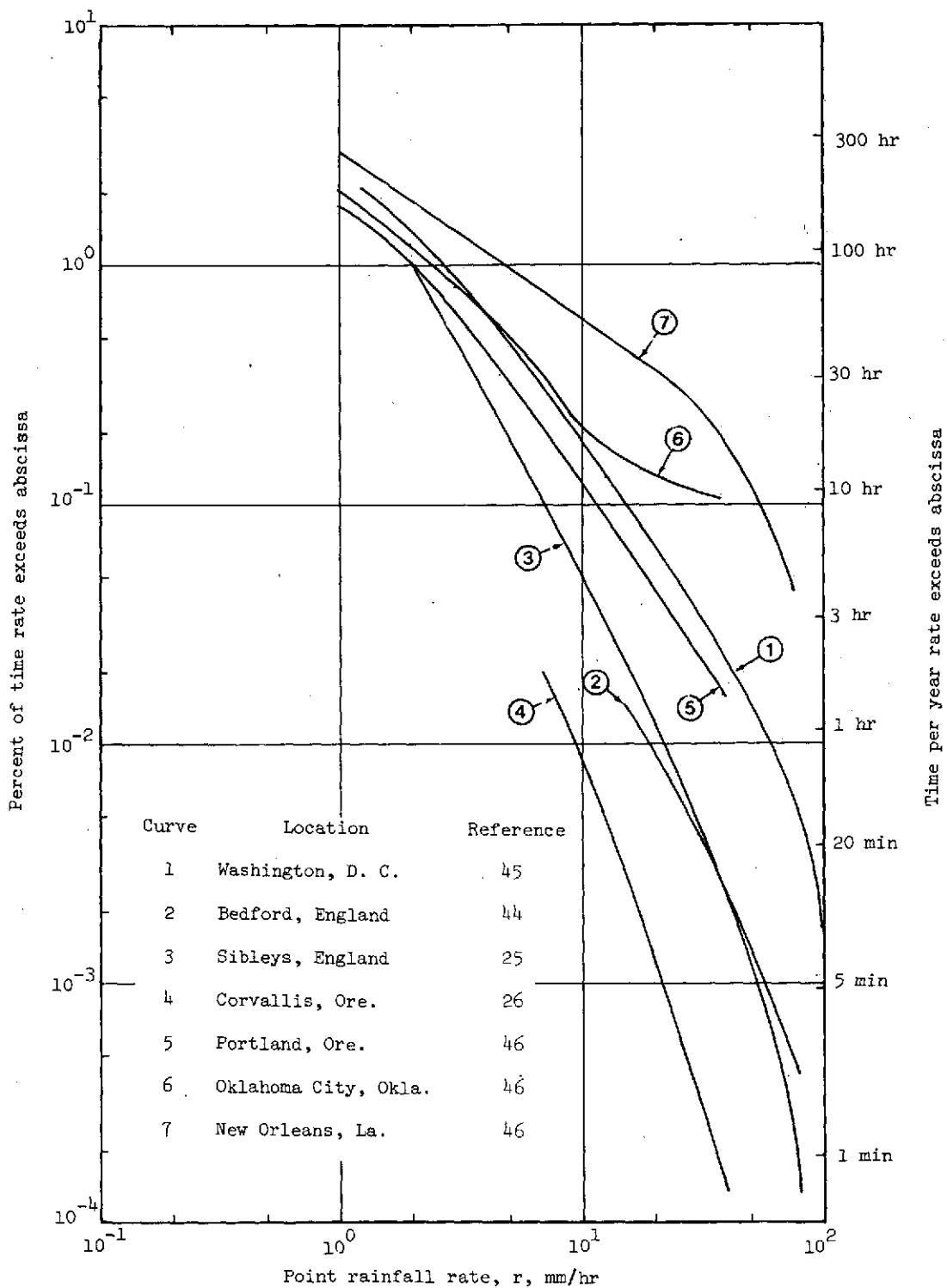Figure 28.- Maximum clutter limited range in rain.

Figure 29.- Frequency of occurrence of rainfall.

Snow

The published information concerning the attenuation and reflection of electromagnetic waves by snow is much more incomplete than for rain. From Gunn and East (ref. 36) the attenuation by dry snow falling at a rate of 3 mm of water per hr is calculated to be 2.5×10^{-3}, 4.6×10^{-3}, and 4.5×10^{-2} dB/km at 10, 15, and 35 GHz, respectively. A few measurements have been made which indicate a much greater attenuation coefficient. Bell (ref. 48) has measured the coefficient to be 0.45 dB/km at 11 GHz for a rate of 2 mm of water per hr. Oomori and Aoyagi (ref. 49) measured the attenuation to be approximately 0.27, 0.70, and 1.6 dB/km at 10, 15, and 35 GHz, respectively. It is possible that the higher measured values are due to the snow being wet and thus having a higher dielectric constant. If this is true, then the above data indicate that attenuation due to dry snow would not be a serious problem for the radar imaging ILM. Wet snow could degrade the performance at 35 GHz such that the system would be inadequate.

The theoretical reflectivities from reference 36 are -70.6, -63.6, and -48.9 dB/m at 10, 15, and 35 GHz, respectively, for a snowfall rate of 3 mm/hr. Measurements by Carlson (ref. 50) indicate higher reflectivities of -58.5, -51.5, and -36.8 dB/m, all for linear polarization. From table VI the reduction in reflectivity with circular polarization is 12 to 26 dB. The scarcity of data seems to make exact computations of the maximum clutter limited range of questionable value. However, comparison of the above quoted values for the measured reflectivity of snow with the comparable data for rain in figures 26 and 28 indicates possible serious degradation in performance due to clutter, particularly at 35 GHz.

Fog

Microwave attenuation by fog has been described theoretically in the classical work by Gunn and East (ref. 36). Using Rayleigh scattering theory they found that the attenuation coefficient α is given by

$$\alpha = 0.4343 \frac{6\pi M}{\lambda \rho_W} \text{Im}(-K) \tag{77}$$

where

α attenuation coefficient, dB/km

M   mass of condensed water per unit volume of air, g/m^3

λ wavelength, cm

ρ_W density of water, g/cm^3

60

$$K = \frac{m^2 - 1}{m^2 + 2}$$

m   complex refractive index

The resulting values for α at a temperature of 0^0 C are plotted in figure 30 as a function of M for the three frequencies of interest. The temperature of 0^0 C was chosen to be conservative, since the attenuation increases (because of the dielectric constant) with decreasing temperature.
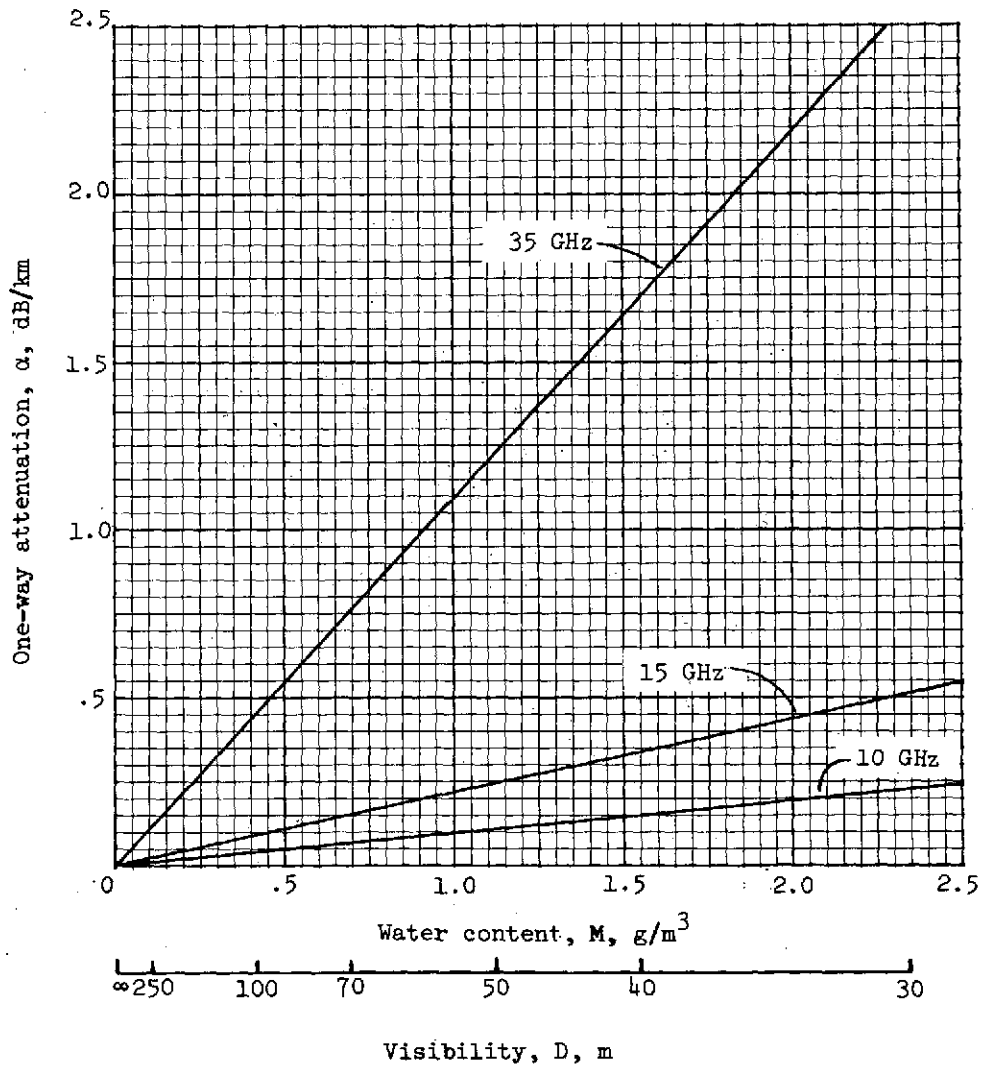

Figure 30.- Attenuation in fog.

A second abscissa scale in terms of the visibility distance D is shown in figure 30. The following relationship between M and D was taken from Kerr (ref. 51):

$$M = 303D^{-1.43} \tag{78}$$

where D is visibility in feet.

Using the same limits for target cross section σ_0 used in figures 24 and 28, values of the attenuation coefficient from figure 30, and 15 dB for the required SNR, the maximum attenuation limited range in fog was computed using equation (69) for a 1.57 m antenna. The results are shown graphically in figure 31.
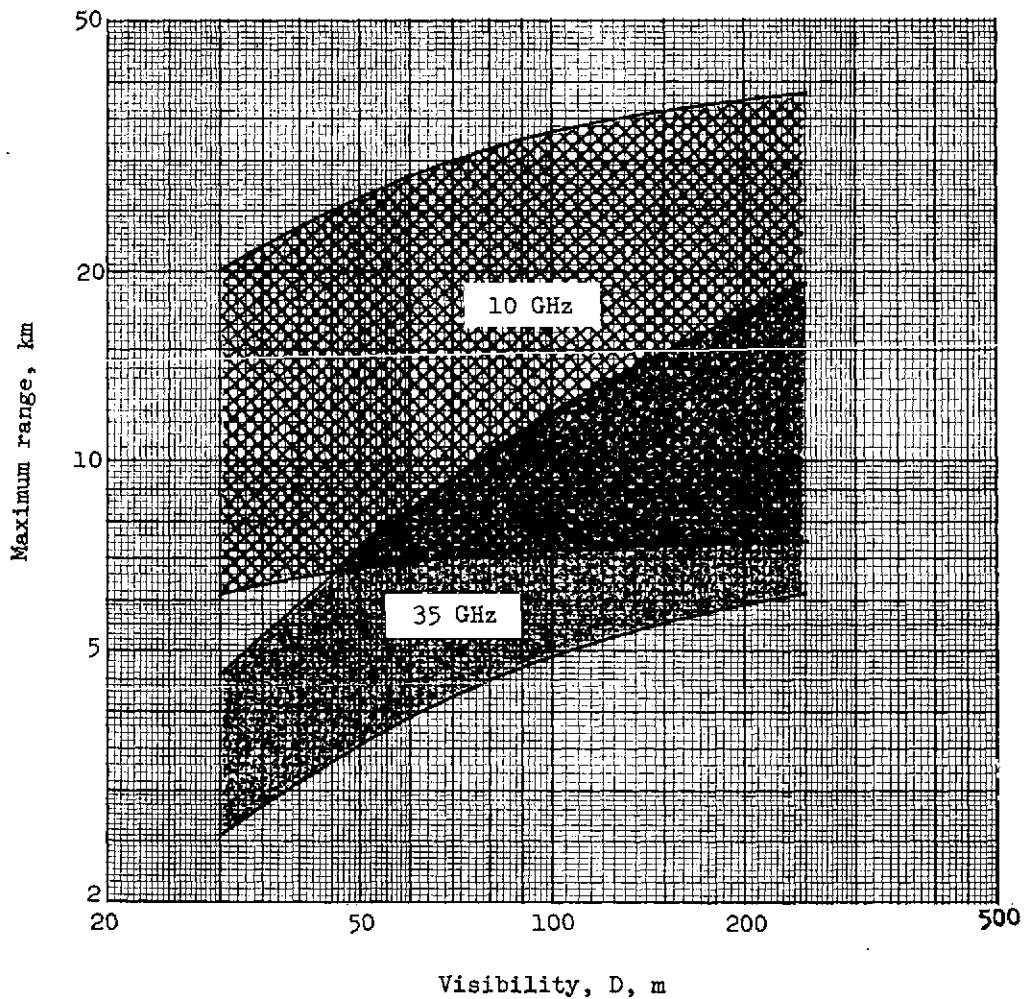

Figure 31.- Maximum attenuation limited range in fog.

From the standpoint of attenuation, the baseline system at 10 GHz can operate satisfactorily in fog in which the visibility is 30 m or more. At 35 GHz the system can operate in fog with a visibility of 200 m and perhaps with a visibility of 40 m. This performance may be adequate in view of Kerr's statement (ref. 51) that fog seldom occurs with a water content of more than 1 g/m^3, which corresponds to a visibility of about 55 m. Furthermore, one author (ref. 5) has stated that reduction of landing minimums to 150 m visibility will be an adequate solution to the problem of airline operation in poor weather.

Gunn and East (ref. 36) and Skolnik (ref. 6) give theoretical values for the backscatter cross section of fog. At 35 GHz and 0° C the relationship between reflectivity and water content from Gunn and East is

$$\Sigma = 1.47 \times 10^{-9} M^{1.82} \tag{79}$$

For M = 2.3 g/m^3, corresponding to a visibility of about 30.48 m (100 ft), Σ = -81.7 dB/m for linear polarization. Due to the high spherical symmetry of the droplets in fog, the cancellation ratio for circular polarization should be limited only by the ellipticity of the radar system. Assuming a value of 25 dB for the cancellation ratio, the reflectivity for this worst case becomes -106.7 dB/m. From equation (76) the corresponding maximum clutter limited range is nearly 9000 km for σ_O = -36 dBsm. Therefore, it is concluded that fog clutter is not a problem for the radar imaging ILM.

CONCLUSIONS

From the analysis of a real aperture, forward-looking imaging radar for use as an independent landing monitor (ILM), the following results have been obtained:

1. The requirements on ground resolution, signal-to-noise ratio, signal-to-clutter ratio, maximum range, and weather environment have not been established for an imaging type ILM.

So that the capabilities of a radar imager could be evaluated, the following requirements were assumed or heuristically derived: (1) ground resolution of 23 m at maximum range, (2) signal-to-noise ratio of 15 dB (postdetection), (3) maximum range of 6 km, and (4) all weather environments. It must be emphasized that some of the following conclusions are based on the foregoing assumptions and that any revision in the assumed requirements could change the conclusions.

2. The selection of the operating frequency for a radar imaging ILM involves a trade-off between cross-track resolution and performance in adverse weather, particularly rain. Higher frequencies produce better cross-track resolution, while lower frequencies produce less weather degradation. Also involved in the trade-off is antenna length, where longer antennas afford improved cross-track resolution.

3. At a range of 6 km and with a 2 m antenna, an imaging radar ILM operating at a frequency of 35 GHz will have a cross-track resolution of 25.7 m (84.3 ft), which nearly satisfies the assumed resolution requirement of 23 m and probably is adequate. The resolution of a 35 GHz imager with a 1.57 m antenna is 32.8 m (108 ft) and does not satisfy the requirement but may be adequate. The resolutions at 35 GHz with a 0.761 m (30 in.) antenna, at 15 GHz with a 2 m antenna, and at 10 GHz with a 2 m antenna are 67.8 m, 60.0 m, and 90.0 m, respectively, at a range of 6 km and do not nearly meet the requirement.

Even if the maximum range could be reduced to 4.25 km, corresponding to the range to the far end of a 3.66 km (12 000 ft) runway, from an aircraft altitude of 30.5 m (100 ft), radar imaging ILM's operating at 10 GHz or 15 GHz do not meet the 23 m resolution requirement with antenna lengths up to 2 m. If a cross-track resolution equal to the runway width (typically 45.7 m) were acceptable, then a radar imager at 15 GHz with a 2 m antenna would be adequate since it has a resolution of 42.5 m. Adequate cross-track resolution can be obtained at 10 GHz or 15 GHz only if the assumed resolution requirements are relaxed or if antennas longer than 2 m can be accommodated by the aircraft (such as in the wings).

4. Adequate signal-to-noise ratios from a grass-surrounded runway can be obtained at ranges up to 6 km in clear weather.

5. Because the measured values of the differential radar cross section of concrete and undisturbed snow overlap, the performance of a radar imaging ILM with a runway surrounded by snow cannot be predicted and must be determined by testing.

6. Further testing is required to determine the improvements obtainable in image quality through reduction of target clutter by pulse integration.

7. Runway obstructions such as large aircraft and vehicles can be detected with an ILM at a 6 km range. Small aircraft and vehicles can probably be detected at shorter ranges.

8. A radar imaging ILM will not perform satisfactorily in some Category III weather conditions unless antenna lengths greater than 2 m can be accommodated in the aircraft.

9. An X-band radar imaging ILM will not be limited by weather except in the heaviest rains or snows.

10. A radar imaging ILM at 35 GHz will not perform adequately (insufficient range) in moderate rain and may be clutter limited in snow. It will perform satisfactorily in fog except for possible slight attenuation degradation in very heavy fog.

11. A K_a-band radar imaging ILM is feasible if operation in all weather conditions is not mandatory. Further testing must be conducted to determine its limitations and to optimize the design.

12. Circulation polarization should be used to reduce degradation due to weather clutter.

Langley Research Center,
    National Aeronautics and Space Administration,
        Hampton, Va., May 17, 1974.

REFERENCES

1. Bechtel, B.: Radar Independent Landing Monitors. AIAA Paper No. 70-1336, Oct. 1970.

2. Maxson Electronics Div.: Maxson's Independent Landing Monitor. Maxson Electronics Corp., Oct. 1971.

3. Anon.: Results of the Experiments Undertaken on the Landing Function of a New Multi-function Radar. DT.RCM No. 72/955, Thomson-CSF, Oct. 4, 1972.

4. Parks, Donald L.; and Tubb, David G.: Simulator Development and Flight Validation of a Perspective Display as an Independent Landing Monitor. AIAA Paper No. 70-924, July 1970.

5. Schilding, R.: Need and Requirements for the ILM. Electronics and Civil Aviation, Vol. 2, Editions Chiron (Paris), 1972, pp. 928-934.

6. Skolnik, Merrill I., ed.: Radar Handbook. McGraw-Hill Book Co., Inc., c.1970.

7. Cosgriff, R. L.; Peake, W. H.; and Taylor, R. C.: Terrain Scattering Properties for Sensor System Design (Terrain Handbook II). Bull. No. 181, Eng. Exp. Sta., Ohio State Univ. [Stud.], Vol. XXIX, No. 3, May 1960.

8. Grant, C. R.; and Yaplee, B. S.: Back Scattering From Water and Land at Centimeter and Millimeter Wavelengths. Proc. IRE, vol. 45, no. 7, July 1957, pp. 976-882.

9. Hoekstra, Pieter; and Spanogle, Dennis: Backscatter From Snow and Ice Surfaces at Near Incident Angles. IEEE Trans. Antennas & Propagation, vol. AP-20, no. 6, Nov. 1972, pp. 788-790.

10. Panter, Philip F.: Modulation, Noise, and Spectral Analysis Applied to Information Transmission. McGraw-Hill Book Co., c.1965.

11. Wagenaar, W. A.; and van Meeteren, A.: Noisy Line-Scan Pictures. Photogram. Eng., vol. XXXV, no. 11, Nov. 1969, pp. 1127-1134.

12. Dean, Charles E.: Measurements of the Subjective Effects of Interference in Television Reception. Proc. IRE, vol. 48, no. 6, pt. I, June 1960, pp. 1035-1049.

13. Legault, R. R.: Man — the Final State of an Electro-Optical Imaging System. Electronic and Aerospace Systems Convention Record, IEEE Publ. 69 C 31-AES, Oct. 1969, pp. 16-21.

14. Coltman, J. W.; and Anderson, A. E.: Noise Limitations to Resolving Power in Electronic Imaging. Proc. IRE, vol. 48, no. 5, May 1960, pp. 858-865.

15. Levine, S. H.; Jauer, R. A.; and Kozlowski, D. R.: Human Factors Requirements for Electronic Displays: Effects of S/N and TV Lines-Over-Target. 1970 Proceedings National Aerospace Electronics Conference, IEEE 70-C-14 AES, May 1970, pp. 247-252.

16. Biberman, Lucien M.; Legault, Richard; Milton, A. Fenner; Rosell, Frederick A.; Schade, Otto H., Jr.; Schnitzler, Alvin D.; and Snyder, Harry L.: Image Quality in Sampled Data Systems. Paper P-741, Sci. & Technol. Div., Inst. Def. Anal., Aug. 1971. (Available from DDC as AD 733 663.)

17. Fredendall, Gordon L.; and Behrend, William L.: Picture Quality – Procedures for Evaluating Subjective Effects of Interference. Proc. IRE, vol. 48, no. 6, pt. I, June 1960, pp. 1030-1034.

18. Moore, Richard K.; Waite, William P.; and Rouse, John W., Jr.: Panchromatic and Polypanchromatic Radar. Proc. IEEE, vol. 57, no. 4, Apr. 1969, pp. 590-593.

19. Waite, William P.: Broad-Spectrum Electromagnetic Backscatter. CRES Tech. Rep. No. 133-17 (Contract Nos. DAAK 02-68-C-0089 and NAS 9-10261), Univ. of Kansas, Aug. 1970. (Available as NASA CR-117035.)

20. Cram, L. A.: Modelling Methods of Determining Radar Echo Characteristics. Determination and Use of Radar Scattering Characteristics, AGARD-LS-59, Sept. 1973, pp. 1(e)-1 – 1(e)-7.

21. Woolcock, S. C.: Use of Radio Modelling Data. Determination and Use of Radar Scattering Characteristics, AGARD-LS-59, Sept. 1973, pp. 3(b)-1 – 3(b)-13.

22. Medhurst, Richard G.: Rainfall Attenuation of Centimeter Waves: Comparison of Theory and Measurement. IEEE Trans. Antennas & Propagation, vol. AP-13, no. 4, July 1965, pp. 550-564.

23. Harrold, T. W.: Attenuation of 8.6 mm-Wavelength Radiation in Rain. Proc. Inst. Elec. Eng. (London), vol. 114, no. 2, Feb. 1967, pp. 201-203.

24. Blevis, Bertram C.; Dohoo, Ray M.; and McCormick, K. Stewart: Measurements of Rainfall Attenuation at 8 and 15 GHz. IEEE Trans. Antennas & Propagation, vol. AP-15, no. 3, May 1967, pp. 394-403.

25. Easterbrook, B. J.; and Turner, D.: Prediction of Attenuation by Rainfall in the 10.7 – 11.7 GHz Communication Band. Proc. Inst. Elec. Eng. (London), vol. 114, no. 5, May 1967, pp. 557-565.

26. Hogg, D. C.: Statistics on Attenuation of Microwaves by Intense Rain. Bell Syst. Tech. J., vol. 48, no. 9, Nov. 1969, pp. 2949-2962.

27. Ippolito, Louis J.: Millimeter Wave Propagation Measurements From the Applications Technology Satellite (ATS-V). IEEE Trans. Antennas & Propagation, vol. AP-18, no. 4, July 1970, pp. 535-552.

28. Semplak, R. A.: The Influence of Heavy Rainfall on Attenuation at 18.5 and 30.9 GHz. IEEE Trans. Antennas & Propagation, vol. AP-18, no. 4, July 1970, pp. 507-511.

29. Roche, James F.; Lake, Herman; Worthington, Donald T.; Tsao, Carson K. H.; and deBettencourt, Joseph T.: Radio Propagation at 27-40 GHz. IEEE Trans. Antennas & Propagation, vol. AP-18, no. 4, July 1970, pp. 452-462.

30. Godard, Serge L.: Propagation of Centimeter and Millimeter Wavelengths Through Precipitation. IEEE Trans. Antennas & Propagation, vol. AP-18, no. 4, July 1970, pp. 530-534.

31. Crane, R. K.: Propagation Phenomena Affecting Satellite Communication Systems Operating in the Centimeter and Millimeter Wavelength Bands. Proc. IEEE, vol. 59, no. 2, Feb. 1971, pp. 173-188.

32. Semplak, R. A.: Dual Frequency Measurements of Rain-Induced Microwave Attenuation on a 2.6-Kilometer Propagation Path. Bell Syst. Tech. J., vol. 50, no. 8, Oct. 1971, pp. 2599-2606.

33. Crane, R. K.: Microwave Scattering Parameters for New England Rain. ESD-TR-66-447, U.S. Air Force, Oct. 3, 1966. (Available from DDC as AD 647 798.)

34. Mueller, E. A.; and Sims, A. L.: Relationships Between Reflectivity, Attenuation, and Rainfall Rate Derived From Drop Size Spectra. ECOM 02071-F, U.S. Army, May 1969. (Available from DDC as AD 853 364.)

35. Wexler, Raymond; and Atlas, David: Radar Reflectivity and Attenuation of Rain. J. Appl. Meteorol., vol. 2, no. 1, Feb. 1963, pp. 276-280.

36. Gunn, K. L. S.; and East, T. W. R.: The Microwave Properties of Precipitation Particles. Quart. J. Ray. Meteorol. Soc., vol. 80, no. 346, Oct. 1954, pp. 522-545.

37. Wheeler, M. S.; and Badertscher, K. A.: Radar Mapping in Heavy Rain With Orthogonal Radar Modes at X-band and K_A-Band. 1970 Proceedings National Aerospace Electronics Conference, IEEE 70-C-14-AES, May 1970, pp. 72-80.

38. Nathanson, Fred E.: Radar Design Principles. McGraw-Hill Book Co., Inc., 1969.

39. Gent, H.; Hunter, I. M.; and Robinson, N. P.: Polarization of Radar Echoes, Including Aircraft, Precipitation and Terrain. Proc. IEE, vol. 110, no. 12, Dec. 1963, pp. 2139-2148.

40. Newell, Reginald E.; Geotis, Spiros G.; Stone, Melvin L.; and Fleisher, Aaron: How Round are Raindrops? Proceedings Fifth Weather Radar Conference and 139th National Meeting of the A.M.S., Signal Corps Eng. Lab., Sept. 1955, pp. 261-268.

41. Panasiewicz, Joseph J.: Enhancement of Aircraft Radar Return by Use of Airborne Reflectors and Circular Polarization. IRE Conv. Record, vol. 4, pt. 8, 1956, pp. 89-96.

42. McFee, R.; and Maher, T. M.: Effect of Surface Reflections on Rain Cancellation of Circularly Polarized Radars. IRE Trans. Antennas & Propagation, vol. AP-7, no. 2, Apr. 1959, pp. 199-201.

43. Beasley, Eric W.: Effect of Surface Reflections on Rain Cancellation in Radars Using Circular Polarization. Proc. IEEE, vol. 54, no. 12, Dec. 1966, pp. 2000-2001.

44. Hogg, D. C.: Path Diversity in Propagation of Millimeter Waves Through Rain. IEEE Trans. Antennas & Propagation, vol. AP-15, no. 3, May 1967, pp. 410-415.

45. Weibel, Gerhard E.; and Dressel, Herman O.: Propagation Studies in Millimeter-Wave Link Systems. Proc. IEEE, vol. 55, no. 4, Apr. 1967, pp. 497-513.

46. Cole, A. E.; Donaldson, R. J.; Dyer, R.; Kantor, A. J.; and Skrivanek, R. A.: Precipitation and Clouds: A Revision of Chapter 5, Handbook of Geophysics and Space Environments. AFCRL-AFSG-212, U.S. Air Force, Nov. 1969. (Available from DDC as AD 703 288.)

47. Jasik, Henry, ed.: Antenna Engineering Handbook. First ed., McGraw-Hill Book Co., Inc., c.1961.

48. Bell, J.: Propagation Measurements at 3.6 and 11 Gc/s Over a Line-of-Sight Radio Path. Proc. Inst. Elec. Eng. (London), vol. 114, no. 5, May 1967, pp. 545-549.

49. Oomori, Takeo; and Aoyagi, Syozo: A Presumptive Formula for Snowfall Attenuation of Radio Waves. Electron. and Commun. Japan, vol. 54-B, no. 9, Sept. 1971, pp. 34-39.

50. Carlson, Paul E.: Measurement of Snowfall by Radar. AFCRL 68 0184, U.S. Air Force, Mar. 1968. (Available from DDC as AD 671 941.)

51. Kerr, Donald E., ed.: Propagation of Short Radio Waves. Boston Tech. Publ., Inc., 1964.